A heme-binding domain controls regulation of ATP-dependent potassium channels

Mark J. Burton[a,1], Sofia M. Kapetanaki[b,1], Tatyana Chernova[c], Andrew G. Jamieson[b], Pierre Dorlet[d], Jérôme Santolini[d], Peter C. E. Moody[e], John S. Mitcheson[a], Noel W. Davies[a], Ralf Schmid[a], Emma L. Raven[b,2], Nina M. Storey[a,2]

[a] Department of Molecular and Cell Biology, University of Leicester, Leicester, LE1 9HN, United Kingdom.

[b] Department of Chemistry, University of Leicester, Leicester, LE1 7RH, United Kingdom.

[c] MRC Toxicology Unit, Hodgkin Building, Lancaster Road, Leicester LE1 9HN, United Kingdom.

[d] Institute for Integrative Biology of the Cell (I2BC), CEA, CNRS, Univ Paris-Sud, Université Paris-Saclay, 91198, Gif-sur-Yvette cedex, France.

[e] Department of Molecular and Cell Biology and Henry Wellcome Laboratories for Structural Biology, University of Leicester, Leicester, LE1 9HN, United Kingdom.

CLASSIFICATION: Biological sciences, biochemistry.

Author contributions: A.G.J., N.W.D., J.S.M., P.C.E.M., E.L.R and N.M.S. designed research; M.J.B., S.M.K., T. C., P.D., J.S. and N.M.S performed the experiments; M.J.B., S.M.K., P.D., J.S. N.W.D., J.S.M., R.S., P.C.E.M., E.L.R and N.M.S. analysed and interpreted data; E.L.R, N.W.D and N.M.S. wrote the paper with contributions from all authors.

[1] These authors contributed equally to this work.

[2] To whom correspondence should be addressed. Email: emma.raven@le.ac.uk or ns140@le.ac.uk.

Abstract

Heme iron has many and varied roles in biology. Most commonly it binds as a prosthetic group to proteins, and it has been widely supposed and amply demonstrated that subtle variations in the protein structure around the heme, including the heme ligands, are used to control the reactivity of the metal ion. But the role of heme in biology now appears to also include a regulatory responsibility in the cell; this includes regulation of ion channel function. In this work, we show that cardiac K_{ATP} channels are regulated by heme. We identify a cytoplasmic heme-binding $CXXHX_{16}H$ motif on the SUR2A subunit of the channel, and mutagenesis together with quantitative and spectroscopic analyses of heme binding and single channel experiments identified Cys628 and His648 as important for heme binding. We discuss the wider implications of these findings and we use the information to present new hypotheses for mechanisms of heme-dependent regulation across other ion channels.

Significance statement

Heme-containing proteins are found in all living species and carry out a wide variety of biological functions. It is becoming clear that heme has a wider regulatory role in the cell; one such regulatory role is in control of ion channel function. In this paper, we have demonstrated heme-dependent regulation of K_{ATP} channels and we have identified the heme binding location as being on a SUR2A subunit of the channel. We use this information to present a hypothesis for how heme regulation across numerous ion channels may occur.

Keywords

Heme, K_{ATP} channel, heme regulation, SUR2A.

\body

Heme is a small organic molecule with iron in the centre and it plays a vital role in a wide range of biological systems. Heme-containing proteins form a large and biologically important group of enzymes: they are found in all living species and carry out a wide variety of functions, for example in oxygen transport (the globins), electron transfer (the cytochromes), as well as in various heme-dependent catalytic processes (for example in the cytochrome P450s, nitric oxide synthases, peroxidases, dioxygenases). For many of these proteins, much structural and mechanistic information is available, and this has led to an established view that the role of heme in biology is as a prosthetic group, which means that it binds tightly to a particular protein (such as hemoglobin) thus conferring specific properties that vary according to the biological requirements. But it is now becoming clear that this represents only one part of a more complex biological picture and that heme interacts with proteins in a variety of ways and has a much wider regulatory role in the cell (1-5). The mechanisms of heme regulation in biology are, at present, largely unknown.

One new regulatory role for heme is in control of ion channel function. Ion channels are central to the control of a vast range of biological processes ranging from neuronal signaling to regulation of blood pressure, and as a consequence defects in ion channel function lead to a variety of disease states. Ion channel gating (opening and closing of the pore) can be regulated by membrane potential and/or by ligand binding; furthermore, co-assembly with regulatory subunits and modulation by signaling pathways yields an additional means of control.

The molecular basis for the regulatory control in ion channels has yet to be precisely defined. The complexity of the problem is in part because the target proteins and their sites of interaction with heme are poorly characterised and are probably different in different ion channels, and because the interactions with heme are often weak and give spectroscopic signatures that are much different to those in the more well-characterised heme proteins which are often used as a benchmark. Consequently, the development of ideas about precisely how heme regulates such complex biological events is at a preliminary stage, and the mechanisms of regulation in structurally diverse channels have yet to be unravelled.

In this paper, we have examined heme-dependent regulation in cardiac ATP-sensitive K^+ channels (K_{ATP}). K_{ATP} channels regulate the excitability of cardiac ventricular myocytes which is especially apparent during metabolic stress, such as, ischaemic heart disease and myocardial infarction (6). We find clear evidence for heme-dependent modulation of cardiac K_{ATP} channels and our analyses indicate that heme interacts with a cytoplasmic regulatory domain to modulate channel activity. We use this

information to present a mechanistic framework for heme-dependent regulation across other ion channels.

Results

The K_{ATP} family of ion channels respond to intracellular ATP and play a pivotal role in linking cellular metabolism to excitability (7). The most abundant ventricular K_{ATP} channel is a heteroctomeric complex consisting of four pore forming K^+ channel subunits of the inward rectifier family (Kir6.2) and four regulatory sulphonylurea receptor subunits (SUR2A) which are members of the ABC transporter superfamily (8, 9), Fig. S1*A*. The modulation of K_{ATP} channel activity is an important process which enhances the cardiac muscle response to oxidative stress (10).

Heme increases whole-cell K_{ATP} currents. The effect of heme on the K_{ATP} current from isolated cardiac myocytes was investigated using whole-cell patch-clamp recordings. Cardiac myocytes were held at 0 mV and bath application of the K_{ATP} channel opener, P1075 (10 μM), resulted in a whole-cell current which was sensitive to bath application of the selective K_{ATP} channel blocker, glibenclamide (10 μM), that completely blocked the current (Fig. S2*A*). The application of heme (500 nM) resulted in an increase in the K_{ATP} current, producing a 1.6 fold increase in K_{ATP} current (Figs. S2*B*, *C*). Heme increased the K_{ATP} current in a dose dependent manner with a maximal response achieved with 500 nM heme; the half maximal increase in K_{ATP} channel open probability in response to heme is ~100 nM, Fig. S2*C*, which is in the physiological range for heme concentration within the cell (11). Bath application of protoporphyrin IX (Fig. S2*F*), Zn-protoporphyrin IX (Fig. S2*D, F*) or Sn-protoporphyrin IX (Fig. S2*F*) did not result in any change in the K_{ATP} currents. In further experiments, $FeSO_4$ (500 nM) was superfused onto cardiac myocytes during the recording (Fig. S2*E*). However, in contrast to the heme-induced increases in K_{ATP} current, application of $FeSO_4$ resulted in a significant decrease in K_{ATP} current (Figs. S2*E*, *F*). We conclude that the increases in current are specific to heme, and are not a consequence of the porphyrin ring or iron alone.

Depletion of intracellular free heme reduces K_{ATP} current. The effect of depleting intracellular heme was also tested by incubating myocytes with succinylacetone (SA) which inhibits heme biosynthesis by inhibiting the ALA dehydratase enzyme (the second enzyme in the heme biosynthesis pathway); when intracellular heme levels are decreased a feedback loop causes an increase in expression of aminolevulinate synthase-1 (ALAS-1, the first enzyme in the pathway). After incubation with SA, an increase in the expression of ALAS-1 was observed by Q-PCR (Fig. S3*A*). The K_{ATP} channels were opened by the channel opener P1075 (10 μM) and the resulting currents were recorded from myocytes in the whole-cell configuration. The currents recorded from the myocytes treated with SA (1 mM) for 4 hours were significantly smaller in amplitude compared to the amplitude of control untreated myocytes (Figs. S3*B,C*).

Heme increases cardiac K_{ATP} single channel activity. K_{ATP} channels from ventricular myocytes were recorded in inside-out patches at a holding potential of 70 mV. Immediately after patch excision, the K_{ATP} channel open probability (P_{open}) was high due to lack of ATP in the bath solution (Fig. 1*Ai*). The mean amplitude of single channel currents was approximately 4.5 pA with P_{open} of 0.454 ± 0.063, n = 4 for endogenous K_{ATP} channels in cardiac myocytes. A localised perfusion pipette, enabling rapid solution changes to the intracellular side of the patch, delivered a solution containing ATP (500 µM) directly to the excised patch. The addition of ATP to the patch reduced P_{open} to 0.014 ± 0.009, n = 4 (Fig. 1*Aii,B*). Following this, application of hemin (500 nM) with ATP (500 µM) revealed a significant increase in channel activity, P_{open} to 0.104 ± 0.030, n = 4 (Fig. 1*Aiii,B*).

Identification of the heme binding location. Identification of heme-binding domains within heme-dependent ion channels presents a considerable experimental challenge. The K_{ATP} subunits Kir6.2 and SUR2A do not contain any CXXCH cytochrome *c*-like heme binding motifs, as identified in the BK channels (12). However, SUR2A contains a $CXXHX_{16}H$ motif (nomenclature follows that in (13)), Fig. S1*B*. SUR2A (UniProt id: sp|O60706|ABCC9_HUMAN) is a 1549 residue protein that belongs to the c-subfamily of the ATP-binding cassette (ABC) family, an ABC subfamily also referred to as multidrug resistance-associated proteins (MRP). Based on sequence alignments, SUR2A contains two ATP-binding domains of ABC transporters (Pfam domain id: PF00005) in the regions 684-835 and 1325-1473, and two transmembrane domains of ABC transporters (Pfam domain id: PF00664) in the regions 303-582 and 990-1260, Fig. S1*B*. The $CXXHX_{16}H$ motif of the SUR2A subunit (residues 628-648) is located between the first transmembrane domain and the first nucleotide binding domain, Fig. S1. The hypothesis that the $CXXHX_{16}H$ motif is involved in heme binding was therefore tested by mutagenesis (residues Cys628, His631, His648).

Inside-out patches from HEK293 cells heterologously expressing wild type Kir6.2 and SUR2A show K_{ATP} channel currents with a robust response to heme. In the presence of ATP (500 µM) the K_{ATP} channels had a low open probability (0.023 ± 0.009, n = 9) (Fig. S4*B, C*) compared to the addition of heme (500 nM) when an increase in open probability is observed (0.109 ± 0.020, n = 9) (Fig. S4*B, C*). The increase in open probability was observed over all voltages tested in macropatches (Fig. S4*D*). The channels expressed in HEK293 cells were 4.5pA at 70mV and were sensitive to glibenclamide (50µM) which is indicative of the K_{ATP} channel currents Fig. S4*Aiv*). The effect of mutations in the $CXXHX_{16}H$ motif (at C628S, H631A and H648A) was also tested (Fig. 3). Single channel analysis revealed that both single mutations C628S and H648A had a substantial effect on the K_{ATP} channel response to heme (Fig. 3*A, B*), whereas the H631A mutation had a minor effect on the heme response (Fig. 3*C*). Double and triple mutations showed that any combination of mutations that contained C628S and H648A affected the heme-dependent increases in K_{ATP} channel open probability (Fig. 3*C*). These data are consistent with

the SUR2A subunit of K_{ATP} channel being the site of heme binding, and suggest a role for C628 and H648.

Heme binding to SUR2A. In order to further quantify the interaction of heme with the SUR2A subunit, we examined heme binding to two model peptides as well as to a fragment of the SUR2A subunit (residues S615-L933) containing the entire $CXXHX_{16}H$ region. In assessing the spectroscopic properties of these heme-bound species, it is important to note that the spectra for regulatory heme proteins often differ from those of well-known heme proteins such as the globins and cytochrome *c,* most likely because the heme binds more weakly, and in different orientations.

Peptide A (LPFES**C**KKHTGVQSKPINRKQPGRY**H**LDNYE) contains the residues corresponding to C628/H648. At 1:1 hemin:peptide ratio, peptide A binds heme to form a complex that is clearly red-shifted (λ_{max} = 417 nm, Fig. 4*A*) compared to free hemin (λ_{max} = 385 nm). Similar absorption patterns (λ_{max} = 412-417 nm) have been reported for heme binding to peptides with a single cysteine residue (14) and to proteins with Cys/His coordination (Table S1). Heme binding to a control peptide B (LPFES**S**KK**A**TGVQSKPINRKQPGRF**A**LDNFE) in which Cys and His residues have been replaced did not show any evidence of heme binding under the same conditions.

Additionally, the nucleotide binding domain 1 of SUR2A including the heme binding region (residues S615-L933, Fig. S1*B*) was expressed in *E. coli* and titrated with heme, Fig. 4*B*. The absorption spectrum shows a peak at 413 nm; a similar peak of lower intensity was observed in the absorption spectrum of the H648A mutant. As mentioned above, similar absorption patterns have been reported for heme binding to proteins with Cys/His coordination (Table S1), typical for low-spin type-2 heme thiolate Fe(III) Soret bands (15). Overall, these data are consistent with heme binding to the SUR2A subunit of the K_{ATP} channel, and are in agreement with the electrophysiology data.

Resonance Raman experiments were used to provide further insight on the SUR2A-hemin interaction. In the high-frequency, the spectrum of free hemin displays the distinctive features of a ferric 5-coordinate high-spin complex (5c-HS) with characteristic bands at 1370 cm^{-1} (ν_4), 1490 cm^{-1} (ν_3) and 1571 cm^{-1} (ν_2) (Fig. 4*C*i, Table S2). The ν_{10} mode of 5c-HS heme is hidden by the vinyl stretching bands expected in the 1610-1640 cm^{-1} region (1618 cm^{-1} for the in-plane and 1628 cm^{-1} for the out-of plane vinyl group) (16). When titrated with 0.8 equivalent of hemin, ferric SUR2A(S615-L933) shows significant differences with free hemin (Fig. 4*C*ii), indicating that heme is bound specifically. Besides the bands at 1490 cm^{-1} (ν_3) and 1573 cm^{-1} (ν_2) assigned to a 5c-HS hemin complex that probably originates from some unbound hemin, the ν_4 band shifts to a higher frequency (1373 cm^{-1}) and there are additional bands at 1507 cm^{-1} (ν_3), 1589 cm^{-1} (ν_2) and 1641 cm^{-1} (ν_{10}) that clearly indicate the presence of a 6-coordinate low-spin complex (6c-LS) (Table S2). The proportion of 6c-LS heme is significantly increased when the concentration of SUR2A(S615-L933) is in excess, as indicated by

increases in intensity of the v_3 (1505 cm^{-1}), v_2 (1586 cm^{-1}) and v_{10} (1640 cm^{-1}) bands (Fig. 4Ciii). Time-dependent resonance Raman spectra of the ferric SUR2A(S615-L933)-hemin complex reveal a build-up of the 6c-LS species (Fig. S5), as evidenced by an increase in the intensity of the v_3 (1506 cm^{-1}) and v_{10} (1641 cm^{-1}) bands (Fig. S5ii,iii, Table S2). The spectroscopic data indicate that hemin binding to the channel occurs rapidly, but that complete formation of low-spin heme is slower and presumably involves a conformational rearrangement that 'locks' the heme into place complex. The H648A mutation (Fig. 4*C*iv) leads to a significant decrease of the 6c-LS species compared to the wild type protein (Fig. 4Cii) as indicated by the decrease of the intensity of the bands at 1506 cm^{-1} (v_3), at 1590 cm^{-1} (v_2) and 1641 cm^{-1} (v_{10}). These data are consistent with a decreased intensity of the Soret absorbance band at 413nm for the H648A-hemin complex, and with the electrophysiology data. Together, the data suggest that heme binds to SUR2A(S615-L933) at a specific location and that H648 plays a significant role.

EPR data support the conclusions above. The spectrum of the ferric SUR2A(S615-L933)-hemin complex confirms the presence of low-spin heme (g = 2.47, 2.28 and 1.86), Fig. S6ii. As observed in the resonance Raman data above (Fig. 4Ciii), the proportion of 6c-LS heme increases in the presence of higher concentrations of SUR2A, Fig. S6iii. These g-values are typically observed for His-Cys heme ligation, as demonstrated in Fig. S7 (15). Some high-spin heme is visible (g = 6, Fig. S4ii), which probably arises from a small amount of free hemin (compare Fig. S6i). EPR data show that the 6c-LS signals essentially disappear in the H648A mutant (Fig. S6iii), in agreement with the resonance Raman spectra (Fig. 4Civ), and confirming the importance of this residue in heme binding. The mutation of the C628S residue had less of an impact on the EPR spectra (Fig. S6v) (resonance Raman data for C628S showed a similar pattern), but mutation of H631 decreases the amount of 6c-LS species (Fig. S6vi). The implications of these findings are discussed below.

Discussion

Most of what is known about the role of heme iron in biology has emerged over many decades from structure/function studies on well-known heme proteins, for example the globins, the cytochromes, and the many and varied catalytic heme enzymes. But there is evidence in the literature that heme acts as a signalling molecule and also regulates a variety of other complex biological events in the cell, which extends the role of heme far beyond the limits of current understanding. As well as roles in control of ion channel function, there is very good evidence for the involvement of heme in circadian control (day/night cycle), in control of transcriptional events and gene expression, and in regulation of phosphorylation and kinase activity (see (1, 3, 17, 18) for reviews).

The mechanisms of heme-dependent regulation are very unclear. It is not yet known how heme is stored and mobilized within the cell for regulatory control: heme is insoluble in aqueous solutions, and is most likely bound (weakly) to as yet unknown chaperone/transporter proteins, but the mechanisms of heme transport across the membrane are not established in detail. Heme concentrations in the cell have not been measured precisely (estimates are in the range ≈100 nM or less (4, 11, 19), and probably increase during hypoxia and after thrombosis/stroke (20-22) so that local changes in heme concentration in the cell cannot, at present, be reliably quantified.

Heme binding interactions in ion channels. In the case of ion channel regulation, it has recently emerged that there is a role for heme (12, 23-26), but the observations are largely empirical, so that the molecular basis for the regulatory control within individual channel proteins has yet to be properly defined. A number of heme responsive motifs (27) have been suggested to be involved: these include Cys/Pro (CP) motifs using thiolate ligation to the heme as in the P450s, or Cys/His motifs (3, 14). In the case of the Slo1 channels (12), a cytochrome *c*-like CXXCH motif has been implicated (12, 28). But this raises immediate questions that do not chime with established patterns of behavior in other heme proteins, This is because most proteins bind heme reversibly (*i.e.* non-covalently), whereas cytochrome *c* uses complex and specialized biosynthetic machinery to bind heme irreversibly (*i.e.* covalently) through thioether bonds from the Cys residues of the CXXCH motif to the heme vinyl groups (29, 30). There is as yet no evidence that ion channels proteins use similarly specialised biosynthetic machinery; thus, it seems unlikely that the heme is covalently attached. Neither the epithelial sodium channels (24) nor the A-type K^+ channels (23) contain a CXXCH motif, which we interpret to mean that the mode of heme binding is most likely not the same across all ion channels.

In this paper, we have quantified the effect of heme on ATP-dependent potassium channels. These channels couple electrical activity at the membrane to energy metabolism in numerous cells, such as pancreatic β cells and cardiac myocytes, and in this way regulate a number of key physiological

processes including secretion and muscle contraction. We showed that heme at physiological concentrations is a robust activator of K_{ATP} channels, Figs S1, 2. We identified a $CXXHX_{16}H$ heme binding motif on the SUR2A domain as a potential heme binding location. Quantitative analyses of heme binding to model peptides as well as to a fragment of the SUR2A subunit expressed in *E. coli* demonstrate that heme binds to SUR2A(S615-L933), specifically, at this location. At least as far as the isolated SUR2A domain is concerned (*i.e.* not within the channel), formation of a low-spin heme species is not instantaneous, and probably occurs after initial formation of a more loosely associated, non-specific heme-protein complex, by a slow conformational transition which "locks" the low-spin SUR2A-hemin complex in place. Mutagenesis, together with single channel data, implicate Cys628 and His648 as involved in the heme regulatory response, Fig. 3. The spectroscopic data are clearly consistent with His648 as a potential ligand to a low-spin heme species which, on the basis of EPR g-values (Fig. S7), we have tentatively assigned as His/Cys ligated species. Our spectroscopic data for the Cys628 variant do not unambiguously confirm this residue as a ligand to the low-spin heme species, even though a role for Cys628 is clearly evident from the single channel electrophysiology data. Other heme binding modes are most likely possible (as also indicated by our findings on the H631 mutant), so that alternative residues may bind to the heme in the absence of Cys628. Such flexibility of heme binding - particularly flexibility of Cys ligation and particularly redox-linked ligation changes (15) - seems to be a feature of these regulatory heme proteins; it probably reflects an intrinsic mobility of the protein structure (as evidenced by the conformational changes leading to low-spin heme formation) that can, potentially, absorb binding of heme in more than one orientation. A mixture of binding modes have been suggested for the Kv1.4 ball peptide-hemin complex (23).

The $CXXHX_{16}H$ motif (residues 628-648) is located between the first transmembrane domain and the first nucleotide binding domain, Fig. S1. Sequence alignment of the twelve human c-subfamily ABC proteins (Fig. S1*B*) illustrates that the $CXXHX_{16}H$ motif is part of an insertion that is present only in SUR2A and SUR1. SUR1 is the closest homologue to SUR2A (67% identity) within the ABC subfamily c. However, although SUR1 also has the insertion, the $CXXHX_{16}H$ motif is not conserved between SUR2A and SUR1. Hence, this particular mode of heme binding is specific to SUR2A, and does not occur in other members of this family of ABC transporters. There is evidence for heme binding to ABC-transporter proteins (31-35) in other (unrelated) heme transport systems, but the heme binding sites are not established.

Looking at all the heme-dependent ion channels identified so far, we note that cysteine is implicated as important for heme binding in all cases (Table S1). There is, as yet, no structural information on how heme binds to any ion channel protein. Modelling of SUR2A based on the crystal structure (36) of the homologue MRP1 from *C. elegans* illustrates the orientation of the two transmembrane and

two nucleotide binding domains, Fig. 2. The region containing the $CXXHX_{16}H$ motif cannot be modelled meaningfully (and might be conformationally mobile) because this insertion is missing in MRP1 *C. elegans,* but the model indicates that the heme binding region is close to the first nucleotide binding domain (NBD1, Fig. 2*A, B*). In this regard, there are similarities to the structure of human Slo1, because the proposed CXXCH heme binding motif in Slo1 is either invisible or only partly visible in crystal structures (37-39), and is thus assumed to be located in an unstructured (conformationally mobile) region of the molecule.

Consideration of heme-dependent regulatory mechanisms across other ion channels. To begin to create a framework for the development of ideas on the mechanisms of heme-dependent ion channel regulation, we have summarised schematically the information that has emerged so far for K_{ATP} channels (this work) as well as for Slo1 (BK) (12) and Kv1.4 (23) channels (Scheme 1). In all three channels, we note that the heme interacts with a cytoplasmic domain to modulate channel activity, and in each case the heme is suggested to bind to a flexible region of protein structure. Thus, for the K_{ATP} channels, heme binds to the $CXXHX_{16}H$ motif in the cytoplasmic domain of SUR2A; for the Slo1 (BK) channels, heme binds to the cytochrome *c*-like CXXCH motif in the conformationally mobile region between RCK1 and RCK2 domains; and for the Kv1.4 channel, heme is suggested to bind to a similar $CXXHX_{18}H$ motif close to the N-terminal 'ball and-chain' inactivation domain, which introduces a stable configuration in an otherwise flexible region. Our results indicate that heme binding increases the open channel probability in K_{ATP} channels, but for BK channels the opposite effect is observed and for the Kv 1.4 channels heme binding impairs channel inactivation. Hence, while there may be similarities in the modes of heme binding across different channels, the functional consequences are not the same in each case and are a clear indication of the potential versatility of heme binding processes in ion channel control. Additional layers of biological control can easily be envisaged when one considers that heme concentrations are linked to O_2 concentration by O_2-dependent heme degradation pathways (via heme oxygenase (40)), which itself produces CO. A three-way mechanism of control, linking heme concentrations to O_2 and/or CO binding to heme, could provide considerable versatility around the simple process of heme binding, and would be a neat solution to a conceptually difficult biological problem.

Materials and Methods

Detailed methods on the following subjects are available in *S1 Appendix, SI Materials and Methods*: isolation of cardiac myocytes, transfection and cell culture, electrophysiology, RNA extraction and quantitative real-time PCR analysis, expression and purification of SUR2A NBD1, peptide synthesis, spectroscopy of heme-bound species, bioinformatics analyses, chemicals and reagents, Table S1, Table S2, Figures S1-5.

Acknowledgements

This work was funded by BBSRC grant BB/K000128/1. E.L.R, P.C.E.M. and S.M.K. acknowledge a BBSRC travel grant (BB/M018598/1). We acknowledge the French Infrastructure for Integrated Structural Biology (FRISBI) (ANR-10-INSB-05-01). We thank Mr. C. David Owen (University of St. Andrews) and Dr. David Roper (University of Warwick) for providing the pSUMODAVE vector, Dr. Xiaowen Yang in the Protein Expression Laboratory (PROTEX-University of Leicester) for preparing the SUR2A expression clone in that vector, Dr. Lorenza Francescut for purifying SUR2A vectors and Charlotte Binks for data collection.

Figure legends

Fig. 1. Heme increases K_{ATP} single channel open probabilities. (*A*) (i) K_{ATP} channel currents recorded from an inside-out patch of a ventricular myocyte at +70 mV exposed to normal bath solution containing 0 μM ATP, illustrating high channel activity. (ii) Local perfusion of the same patch with 500 μM ATP reduced channel activity. (iii) Local perfusion of the same patch with 500 μM ATP and 500 nM hemin increased channel activity. (*B*) Overlaid amplitude histograms from the above patch, (fitted with Gaussian distributions) illustrating an increase in single channel activity with application of 500 nM hemin (dashed line).

Fig. 2. (*A*) SUR2A homology model based on *C. elegans* MRP PGP-1. α-helices are displayed as barrels, β-strands as arrows using the colour scheme introduced in Fig. S1*B*. The insert containing the $CXXHX_{16}H$ motif (red) which could not be modelled is schematically indicated as a stretch of residues between the two yellow spheres. (*B*) Zoom into the SUR2A homology model. Visualisation as in (*A*), but only residues that are also present in the multiple sequence alignment in Fig. S1*B* are shown.

Fig. 3. Effect of mutagenesis of the $CXXHX_{16}H$ region of SUR2A on K_{ATP} channel activity. (*A*) Inside-out patch of C628S perfused with 500 μM ATP (*i*), and 500 μM ATP and 500 nM hemin (*ii*), and plots of P_{open} (*iii*) and mean P_{open} (*iv*) with no significant change in activity between 500 μM ATP = 0.053 ± 0.019, n = 7 and 500 μM ATP with 500 nM hemin = 0.043 ± 0.014, n = 7. (*B*) Representative inside-out patch of H648A with 500 μM ATP *(i*), 500 μM ATP and 500 nM hemin (*ii*), all P_{open} values (*iii*) and mean P_{open} (iv): 500 μM ATP = 0.009 ± 0.005, n = 5 and 500 μM ATP with 500 nM hemin = 0.011 ± 0.008, n = 5. (*C*) Mean P_{open} for all mutants; empty bars for 500 μM ATP and hatched bars indicating 500 μM ATP and 500 nM hemin

Fig. 4. Spectroscopic analysis of heme bound to SUR2A and synthetic peptide. (*A*) Spectrophotometric titrations of the synthetic peptide LPFES**C**KKHTGVQSKPINRKQPGRY**H**LDNYE with heme. (*B*) Corresponding heme titration of the SUR2A truncated protein (residues S615-L933) containing the heme binding $CXXHX_{16}H$ region; the arrows represent the directions of the absorbance changes with increasing heme concentration. (*C*) Room temperature high-frequency resonance Raman spectra of (i) hemin, (ii) ferric SUR2A(S615-L933)-hemin at sub stoichiometric hemin concentrations, (iii) ferric SUR2A(S615-L933)-hemin with the protein in 4-5 fold excess, and (iv) H648A-hemin. All spectra collected with 413.1 nm laser excitation.

Scheme 1. Cartoon representation of heme interaction in various ion channels. (*A*) In the K_{ATP} channel (this work), heme binds to the $CXXHX_{16}H$ motif in the unique insertion (G622-P665 in the human protein) on the cytoplasmic domain of SUR2A, and increases the open channel probability. (*B*) In Slo1 (BK) channel (5), heme binds to the cytochrome *c*-like motif CXXCH in the disordered region between the RCK1 and RCK2 domains, and increased concentrations of heme inhibit K^+ currents by decreasing

the frequency of channel opening. Inhibition of channel activity as heme concentration increases is consistent with other observations (41) in which knockdown of heme oxygenase (which would increase heme concentration) also reduces channel activity. (*C*) In the Kv1.4 channel (23), heme binds to the 'ball-and-chain' N-terminus of the A-type potassium channel and impairs the inactivation process; a heme-responsive $CXXHX_{18}H$ motif is suggested as being responsible for heme binding, which introduces a stable configuration in the otherwise disorded region. The membrane is depicted in pale blue and the intracellular side is on the bottom. The light purple rectangles depict the conduction pore of the inward rectifier K^+ channel Kir6.2 subunit in the K_{ATP} channel and the Slo1 and Kv1.4 channels. The grey (TMD0), dark green (TMD1) and light green (TMD2) rectangles represent the transmembrane domains of the sulphonylurea receptor SUR2A in the K_{ATP} channel (colour scheme as in Figure 3), and the dark purple rectangles are the voltage-sensor domains in the Slo1 and Kv1.4 channels. Other transmembrane domains have been omitted for simplicity. NBD: nucleotide binding domains 1 and 2. RCK1/RCK2: regulator of conductance K domains 1 and 2. Heme is depicted as a red diamond.

References

1. Hou S, Reynolds MF, Horrigan FT, Heinemann SH, & Hoshi T (2006) Reversible binding of heme to proteins in cellular signal transduction. *Acc Chem Res* 39(12):918-924.
2. Rodgers KR (1999) Heme-based sensors in biological systems. *Curr Opin Chem Biol* 3(2):158-167.
3. Shimizu T (2012) Binding of cysteine thiolate to the Fe(III) heme complex is critical for the function of heme sensor proteins. *J Inorg Biochem* 108:171-177.
4. Smith AG, Raven EL, & Chernova T (2011) The regulatory role of heme in neurons. *Metallomics : integrated biometal science* 3(10):955-962.
5. Shimizu T*, et al.* (2015) Gaseous O2, NO, and CO in signal transduction: structure and function relationships of heme-based gas sensors and heme-redox sensors. *Chemical reviews* 115(13):6491-6533.
6. Zingman LV, Alekseev AE, Hodgson-Zingman DM, & Terzic A (2007) ATP-sensitive potassium channels: metabolic sensing and cardioprotection. *Journal of applied physiology (1985)* 103(5):1888-1893.
7. Flagg TP, Enkvetchakul D, Koster JC, & Nichols CG (2010) Muscle KATP channels: recent insights to energy sensing and myoprotection. *Physiological reviews* 90(3):799-829.
8. Noma A (1983) ATP-regulated K+ channels in cardiac muscle. *Nature* 305(5930):147-148.
9. Inagaki N*, et al.* (1995) Reconstitution of I-Katp - an Inward Rectifier Subunit Plus the Sulfonylurea Receptor. *Science* 270(5239):1166-1170.
10. Zingman LV*, et al.* (2002) Kir6.2 is required for adaptation to stress. *Proceedings of the National Academy of Sciences of the United States of America* 99(20):13278-13283.
11. Khan AA & Quigley JG (2011) Control of intracellular heme levels: heme transporters and heme oxygenases. *Biochim Biophys Acta* 1813(5):668-682.
12. Tang XD*, et al.* (2003) Haem can bind to and inhibit mammalian calcium-dependent Slo1 BK channels. *Nature* 425(6957):531-535.
13. Bowman SE & Bren KL (2008) The chemistry and biochemistry of heme c: functional bases for covalent attachment. *Nat Prod Rep* 25(6):1118-1130.
14. Kuhl T*, et al.* (2013) Analysis of Fe(III) heme binding to cysteine-containing heme-regulatory motifs in proteins. *ACS chemical biology* 8(8):1785-1793.
15. Smith AT*, et al.* (2015) Functional divergence of heme-thiolate proteins: a classification based on spectroscopic attributes. *Chemical reviews* 115(7):2532-2558.
16. Kalsbeck WA*, et al.* (1996) Structural and electronic properties of the heme cofactors in a multi-heme synthetic cytochrome. *Biochemistry* 35(11):3429-3438.
17. Lukat-Rodgers GS, Correia C, Botuyan MV, Mer G, & Rodgers KR (2010) Heme-based sensing by the mammalian circadian protein CLOCK. *Inorg Chem* 49(14):6349-6365.
18. Gilles-Gonzalez MA & Gonzalez G (2005) Heme-based sensors: defining characteristics, recent developments, and regulatory hypotheses. *J Inorg Biochem* 99(1):1-22.
19. Sassa S (2004) Why heme needs to be degraded to iron, biliverdin IXalpha, and carbon monoxide? *Antioxid Redox Signal* 6(5):819-824.
20. Wagner KR & Dwyer BE (2004) Hematoma removal, heme, and heme oxygenase following hemorrhagic stroke. *Annals of the New York Academy of Sciences* 1012:237-251.
21. Letarte PB*, et al.* (1993) Hemin: levels in experimental subarachnoid hematoma and effects on dissociated vascular smooth-muscle cells. *J Neurosurg* 79(2):252-255.
22. Dore S (2002) Decreased activity of the antioxidant heme oxygenase enzyme: implications in ischemia and in Alzheimer's disease. *Free radical biology & medicine* 32(12):1276-1282.
23. Sahoo N*, et al.* (2013) Heme impairs the ball-and-chain inactivation of potassium channels. *Proc Natl Acad Sci U S A* 110(42):E4036-4044.
24. Wang S, Publicover S, & Gu Y (2009) An oxygen-sensitive mechanism in regulation of epithelial sodium channel. *Proc Natl Acad Sci U S A* 106(8):2957-2962.

25. Hou S, Xu R, Heinemann SH, & Hoshi T (2008) Reciprocal regulation of the Ca2+ and H+ sensitivity in the SLO1 BK channel conferred by the RCK1 domain. *Nat Struct Mol Biol* 15(4):403-410.
26. Hou S, Xu R, Heinemann SH, & Hoshi T (2008) The RCK1 high-affinity Ca2+ sensor confers carbon monoxide sensitivity to Slo1 BK channels. *Proc Natl Acad Sci U S A* 105(10):4039-4043.
27. Kuhl T*, et al.* (2011) Determination of hemin-binding characteristics of proteins by a combinatorial peptide library approach. *Chembiochem : a European journal of chemical biology* 12(18):2846-2855.
28. Yi L, Morgan JT, & Ragsdale SW (2010) Identification of a thiol/disulfide redox switch in the human BK channel that controls its affinity for heme and CO. *J Biol Chem* 285(26):20117-20127.
29. Stevens JM, Daltrop O, Allen JWA, & Ferguson SJ (2004) *C*-type cytochrome formation: chemical and biological enigmas. *Acc. Chem. Res.* 37:999-1007.
30. San Francisco B, Bretsnyder EC, & Kranz RG (2013) Human mitochondrial holocytochrome c synthase's heme binding, maturation determinants, and complex formation with cytochrome c. *Proc Natl Acad Sci U S A* 110(9):E788-797.
31. Woo JS, Zeltina A, Goetz BA, & Locher KP (2012) X-ray structure of the Yersinia pestis heme transporter HmuUV. *Nat Struct Mol Biol* 19(12):1310-1315.
32. Yamashita M*, et al.* (2014) Structure and function of the bacterial heterodimeric ABC transporter CydDC: stimulation of ATPase activity by thiol and heme compounds. *J Biol Chem* 289(33):23177-23188.
33. Chavan H, Khan MM, Tegos G, & Krishnamurthy P (2013) Efficient purification and reconstitution of ATP binding cassette transporter B6 (ABCB6) for functional and structural studies. *J Biol Chem* 288(31):22658-22669.
34. Liesa M, Qiu W, & Shirihai OS (2012) Mitochondrial ABC transporters function: the role of ABCB10 (ABC-me) as a novel player in cellular handling of reactive oxygen species. *Biochim Biophys Acta* 1823(10):1945-1957.
35. Bayeva M*, et al.* (2013) ATP-binding cassette B10 regulates early steps of heme synthesis. *Circ Res* 113(3):279-287.
36. Jin MS, Oldham ML, Zhang Q, & Chen J (2012) Crystal structure of the multidrug transporter P-glycoprotein from Caenorhabditis elegans. *Nature* 490(7421):566-569.
37. Wu Y, Yang Y, Ye S, & Jiang Y (2010) Structure of the gating ring from the human large-conductance Ca(2+)-gated K(+) channel. *Nature* 466(7304):393-397.
38. Yuan P, Leonetti MD, Hsiung Y, & MacKinnon R (2012) Open structure of the Ca2+ gating ring in the high-conductance Ca2+-activated K+ channel. *Nature* 481(7379):94-97.
39. Yuan P, Leonetti MD, Pico AR, Hsiung Y, & MacKinnon R (2010) Structure of the human BK channel Ca2+-activation apparatus at 3.0 A resolution. *Science* 329(5988):182-186.
40. Unno M, Matsui T, & Ikeda-Saito M (2007) Structure and catalytic mechanism of heme oxygenase. *Nat Prod Rep* 24(3):553-570.
41. Williams SE*, et al.* (2004) Hemoxygenase-2 is an oxygen sensor for a calcium-sensitive potassium channel. *Science* 306(5704):2093-2097.
42. Dawson RMC, Elliot DC, Elliot WH, & Jones KM (1975) *Data for Biochemical Research* (Oxford University Press, Oxford, U.K).
43. Lawrence C & Rodrigo GC (1999) A Na+-activated K+ current (I-K,I-Na) is present in guinea-pig but not rat ventricular myocytes. *Pflug Arch Eur J Phy* 437(6):831-838.
44. Chernova T*, et al.* (2007) Neurite degeneration induced by heme deficiency mediated via inhibition of NMDA receptor-dependent extracellular signal-regulated kinase 1/2 activation. *The Journal of neuroscience : the official journal of the Society for Neuroscience* 27(32):8475-8485.
45. Liu H & Naismith JH (2009) A simple and efficient expression and purification system using two newly constructed vectors. *Protein expression and purification* 63(2):102-111.

46. de Araujo ED & Kanelis V (2014) Successful development and use of a thermodynamic stability screen for optimizing the yield of nucleotide binding domains. *Protein expression and purification* 103C:38-47.
47. Aller SG*, et al.* (2009) Structure of P-glycoprotein reveals a molecular basis for poly-specific drug binding. *Science* 323(5922):1718-1722.
48. Gupta N & Ragsdale SW (2011) Thiol-disulfide redox dependence of heme binding and heme ligand switching in nuclear hormone receptor rev-erb{beta}. *J Biol Chem* 286(6):4392-4403.
49. Ishikawa H*, et al.* (2005) Involvement of heme regulatory motif in heme-mediated ubiquitination and degradation of IRP2. *Molecular cell* 19(2):171-181.
50. Qi Z, Hamza I, & O'Brian MR (1999) Heme is an effector molecule for iron-dependent degradation of the bacterial iron response regulator (Irr) protein. *Proc Natl Acad Sci U S A* 96(23):13056-13061.
51. Hirai K*, et al.* (2007) Identification of Cys385 in the isolated kinase insertion domain of heme-regulated eIF2 alpha kinase (HRI) as the heme axial ligand by site-directed mutagenesis and spectral characterization. *J Inorg Biochem* 101(8):1172-1179.
52. Hira S, Tomita T, Matsui T, Igarashi K, & Ikeda-Saito M (2007) Bach1, a heme-dependent transcription factor, reveals presence of multiple heme binding sites with distinct coordination structure. *IUBMB Life* 59(8-9):542-551.
53. Watanabe-Matsui M*, et al.* (2014) Heme binds to an intrinsically disordered region of Bach2 and alters its conformation. *Arch Biochem Biophys* 565C:25-31.
54. Barr I*, et al.* (2011) DiGeorge critical region 8 (DGCR8) is a double-cysteine-ligated heme protein. *J Biol Chem* 286(19):16716-16725.
55. Uchida T*, et al.* (2005) CO-dependent activity-controlling mechanism of heme-containing CO-sensor protein, neuronal PAS domain protein 2. *J Biol Chem* 280(22):21358-21368.
56. Koudo R*, et al.* (2005) Spectroscopic characterization of the isolated heme-bound PAS-B domain of neuronal PAS domain protein 2 associated with circadian rhythms. *FEBS J* 272(16):4153-4162.
57. Mukaiyama Y*, et al.* (2006) Spectroscopic and DNA-binding characterization of the isolated heme-bound basic helix-loop-helix-PAS-A domain of neuronal PAS protein 2 (NPAS2), a transcription activator protein associated with circadian rhythms. *FEBS J* 273(11):2528-2539.
58. Kitanishi K*, et al.* (2008) Heme-binding characteristics of the isolated PAS-A domain of mouse Per2, a transcriptional regulatory factor associated with circadian rhythms. *Biochemistry* 47(23):6157-6168.
59. Hayasaka K, Kitanishi K, Igarashi J, & Shimizu T (2011) Heme-binding characteristics of the isolated PAS-B domain of mouse Per2, a transcriptional regulatory factor associated with circadian rhythms. *Biochim Biophys Acta* 1814(2):326-333.
60. Marvin KA, Kerby RL, Youn H, Roberts GP, & Burstyn JN (2008) The transcription regulator RcoM-2 from Burkholderia xenovorans is a cysteine-ligated hemoprotein that undergoes a redox-mediated ligand switch. *Biochemistry* 47(34):9016-9028.
61. Sono M, Stuehr DJ, Ikeda-Saito M, & Dawson JH (1995) Identification of nitric oxide synthase as a thiolate-ligated heme protein using magnetic circular dichroism spectroscopy. Comparison with cytochrome P-450-CAM and chloroperoxidase. *J Biol Chem* 270(34):19943-19948.
62. Sato A*, et al.* (2002) Stationary and time-resolved resonance Raman spectra of His77 and Met95 mutants of the isolated heme domain of a direct oxygen sensor from Escherichia coli. *J Biol Chem* 277(36):32650-32658.
63. Tomita T, Gonzalez G, Chang AL, Ikeda-Saito M, & Gilles-Gonzalez MA (2002) A comparative resonance Raman analysis of heme-binding PAS domains: heme iron coordination structures of the BjFixL, AxPDEA1, EcDos, and MtDos proteins. *Biochemistry* 41(15):4819-4826.
64. Delgado-Nixon VM, Gonzalez G, & Gilles-Gonzalez MA (2000) Dos, a heme-binding PAS protein from Escherichia coli, is a direct oxygen sensor. *Biochemistry* 39(10):2685-2691.

65. Lukat-Rodgers GS, Rexine JL, & Rodgers KR (1998) Heme speciation in alkaline ferric FixL and possible tyrosine involvement in the signal transduction pathway for regulation of nitrogen fixation. *Biochemistry* 37(39):13543-13552.
66. Gilles-Gonzalez MA*, et al.* (1994) Heme-based sensors, exemplified by the kinase FixL, are a new class of heme protein with distinctive ligand binding and autoxidation. *Biochemistry* 33(26):8067-8073.
67. Rodgers KR, Lukat-Rodgers GS, & Barron JA (1996) Structural basis for ligand discrimination and response initiation in the heme-based oxygen sensor FixL. *Biochemistry* 35(29):9539-9548.
68. Mathews FS (2001) *Handbook of Metalloproteins,*, eds A. Messerschmidt, R. Huber, T.L. Poulos, & Wieghardt K (John Wiley & Sons,, Chichester), Vol 1, pp 159-171.
69. Antonini M & Brunori E (1971) *Hemoglobin and Myoglobin and their Reactions with Ligands* (North Holland Publishers, Amsterdam) pp 10-12.
70. Boffi A, Das TK, della Longa S, Spagnuolo C, & Rousseau DL (1999) Pentacoordinate hemin derivatives in sodium dodecyl sulfate micelles: model systems for the assignment of the fifth ligand in ferric heme proteins. *Biophys J* 77(2):1143-1149.
71. Wood BR*, et al.* (2004) Resonance Raman spectroscopy reveals new insight into the electronic structure of beta-hematin and malaria pigment. *J Am Chem Soc* 126(30):9233-9239.

Figure 1

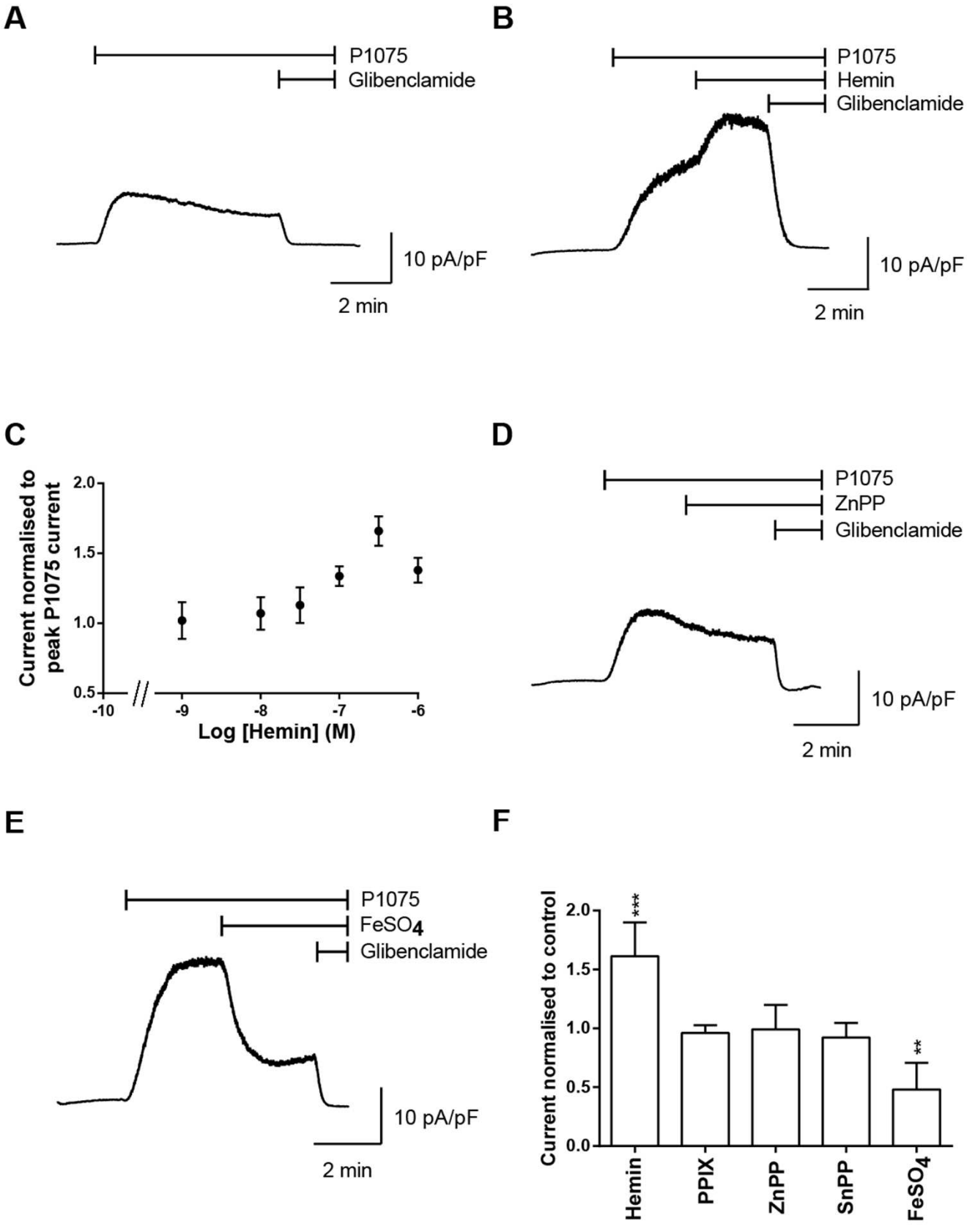
A
P1075
Glibenclamide
10 pA/pF
2 min
B
P1075
Hemin
Glibenclamide
10 pA/pF
2 min
C
Current normalised to peak P1075 current
2.0
1.5
1.0
0.5
-10
-9
-8
-7
-6
Log [Hemin] (M)
D
P1075
ZnPP
Glibenclamide
10 pA/pF
2 min
E
P1075
FeSO4
Glibenclamide
10 pA/pF
2 min
F
Current normalised to control
2.0
1.5
1.0
0.5
0.0
***
**
Hemin
PPIX
ZnPP
SnPP
FeSO4

Figure 2

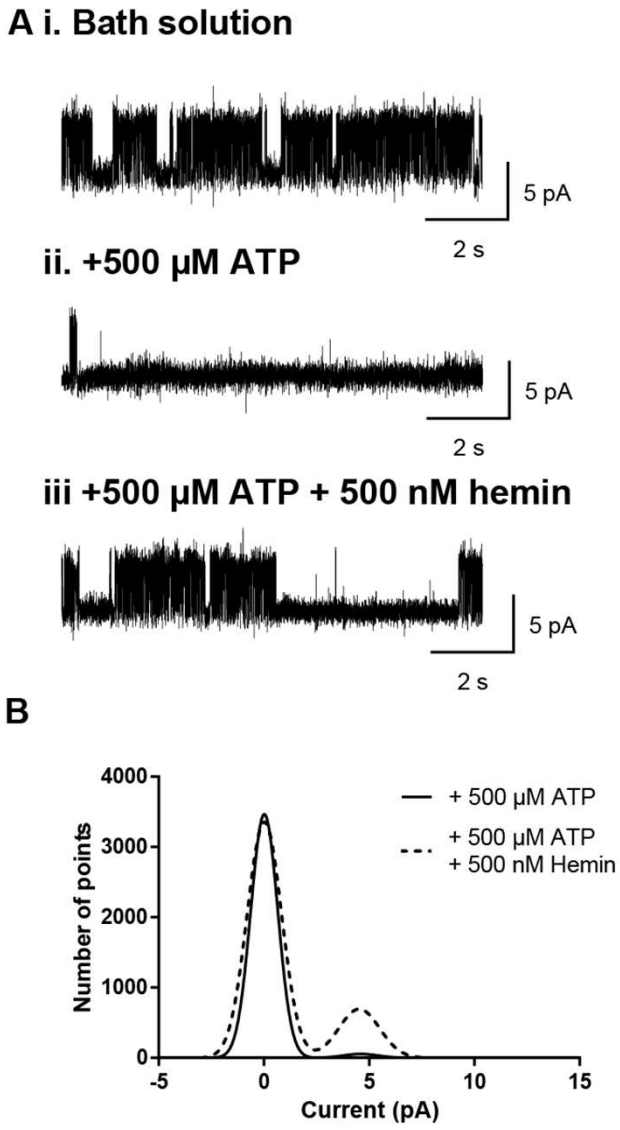
A i. Bath solution
5 pA
2 s
ii. +500 µM ATP
5 pA
2 s
iii +500 µM ATP + 500 nM hemin
5 pA
2 s
B
4000
3000
2000
1000
0
Number of points
-5
0
5
10
15
Current (pA)
+ 500 µM ATP
+ 500 µM ATP
+ 500 nM Hemin

Figure 3

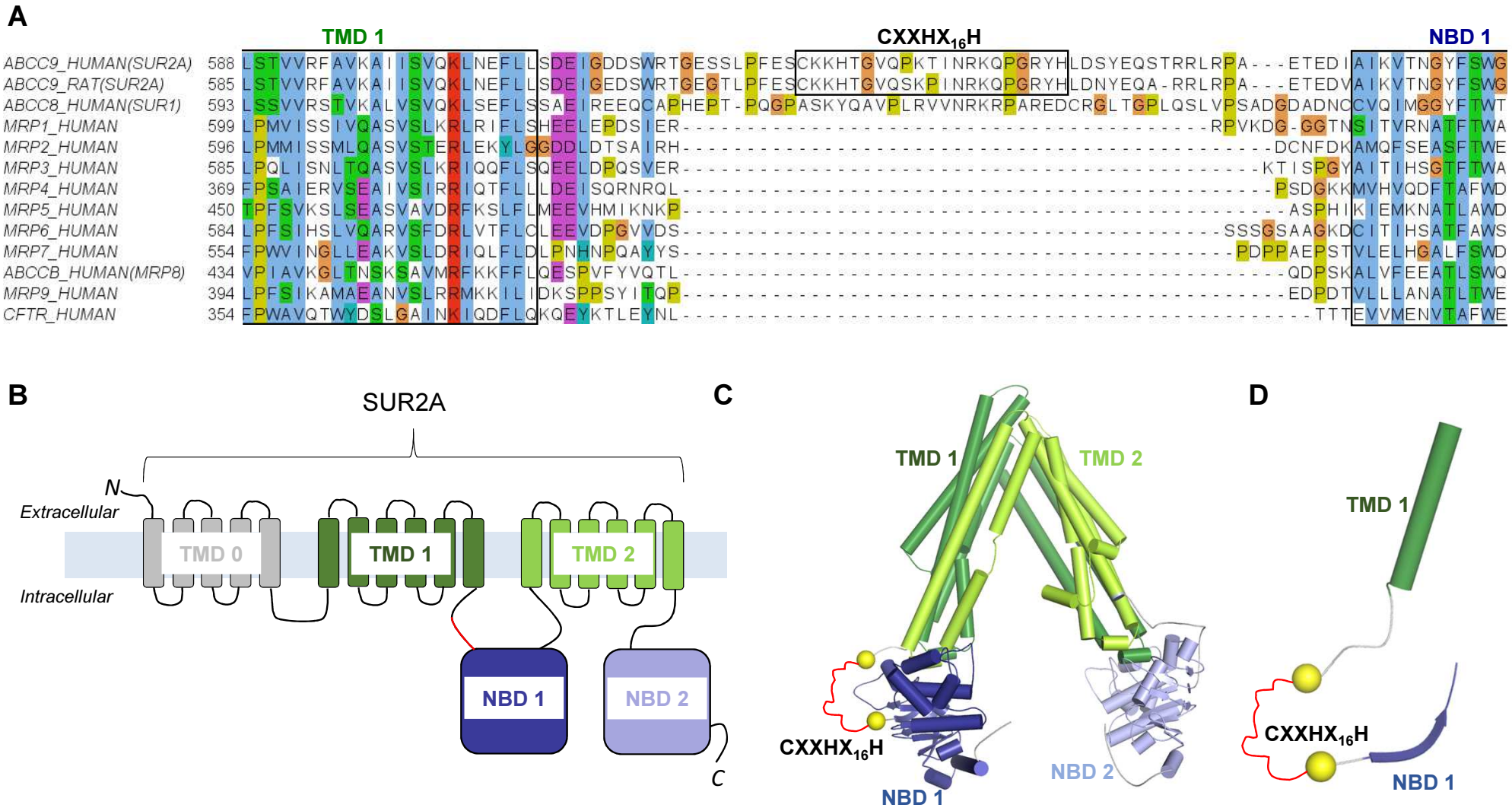
A
TMD 1
CXXHX16H
NBD 1
ABCC9_HUMAN(SUR2A) 588 LSTVVRFAVKAIISVQKLNEFLLSDEIGDDSWRTGESSLPFESCKKHTGVQPKTINRKQPGRYHLDSYEQSTRRLRPA---ETEDIAIKVTNGYFSWG
ABCC9_RAT(SUR2A) 585 LSTVVRFAVKAIISVQKLNEFLLSDEIGEDSWRTGEGTLPFESCKKHTGVQSKPINRKQPGRYHLDNYEQA-RRLRPA---ETEDVAIKVTNGYFSWG
ABCC8_HUMAN(SUR1) 593 LSSVVRSTVKALVSVQKLSEFLSSAEIREEQCAPHEPT-PQGPASKYQAVPLRVVNRKRPAREDCRGLTGPLQSLVPSADGDADNCCVQIMGGYFTWT
MRP1_HUMAN 599 LPMVISSIVQASVSLKRLRIFLSHEELEPDSIER----------RPVKDG-GGTNSITVRNATFTWA
MRP2_HUMAN 596 LPMMISSMLQASVSTERLEKYLGGDDLDTSAIRH----------DCNFDKAMQFSEASFTWE
MRP3_HUMAN 585 LPQLISNLTQASVSLKRIQQFLSQEELDPQSVER----------KTISPGYAITIHSGTFTWA
MRP4_HUMAN 369 FPSAIERVSEAIVSIRRIQTFLLLDEISQRNRQL----------PSDGKKMVHVQDFTAFWD
MRP5_HUMAN 450 TPFSVKSLSEASVAVDRFKSLFLMEEVHMIKNKP----------ASPHIKIEMKNATLAWD
MRP6_HUMAN 584 LPFSIHSLVQARVSFDRLVTFLCLEEVDPGVVDS----------SSSGSAAGKDCITIHSATFAWS
MRP7_HUMAN 554 FPWVINGLLEAKVSLDRIQLFLDLPNHNPQAYYS----------PDPPAEPSTVLELHGALFSWD
ABCCB_HUMAN(MRP8) 434 VPIAVKGLTNSKSAVMRFKKFFLQESPVFYVQTL----------QDPSKALVFEEATLSWQ
MRP9_HUMAN 394 LPFSIKAMAEANVSLRRMKKILIDKSPPSYITQP----------EDPDTVLLLANATLTWE
CFTR_HUMAN 354 FPWAVQTWYDSLGAINKIQDFLQKQEYKTLEYNL----------TTTEVVMENVTAFWE
B
SUR2A
N
Extracellular
Intracellular
TMD 0
TMD 1
TMD 2
NBD 1
NBD 2
C
C
C
TMD 1
TMD 2
CXXHX16H
NBD 1
NBD 2
D
TMD 1
CXXHX16H
NBD 1

Figure 4

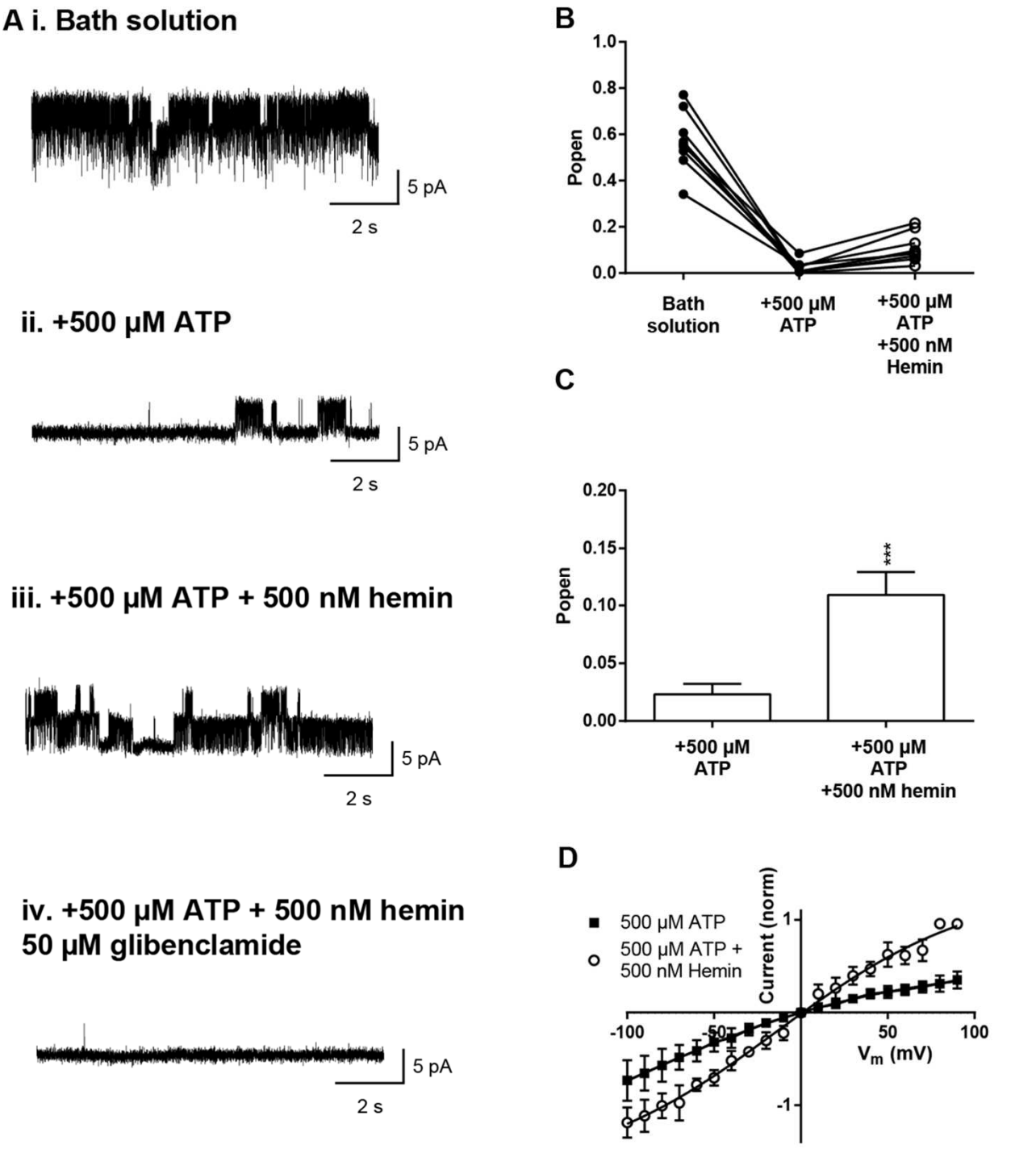
A i. Bath solution
5 pA
2 s
ii. +500 µM ATP
5 pA
2 s
iii. +500 µM ATP + 500 nM hemin
5 pA
2 s
iv. +500 µM ATP + 500 nM hemin
50 µM glibenclamide
5 pA
2 s
B
Popen
1.0
0.8
0.6
0.4
0.2
0.0
Bath solution
+500 µM ATP
+500 µM ATP +500 nM Hemin
C
Popen
0.20
0.15
0.10
0.05
0.00
***
+500 µM ATP
+500 µM ATP +500 nM hemin
D
500 µM ATP
500 µM ATP + 500 nM Hemin
Current (norm)
1
-1
-100
-50
50
100
Vm (mV)

Figure 5

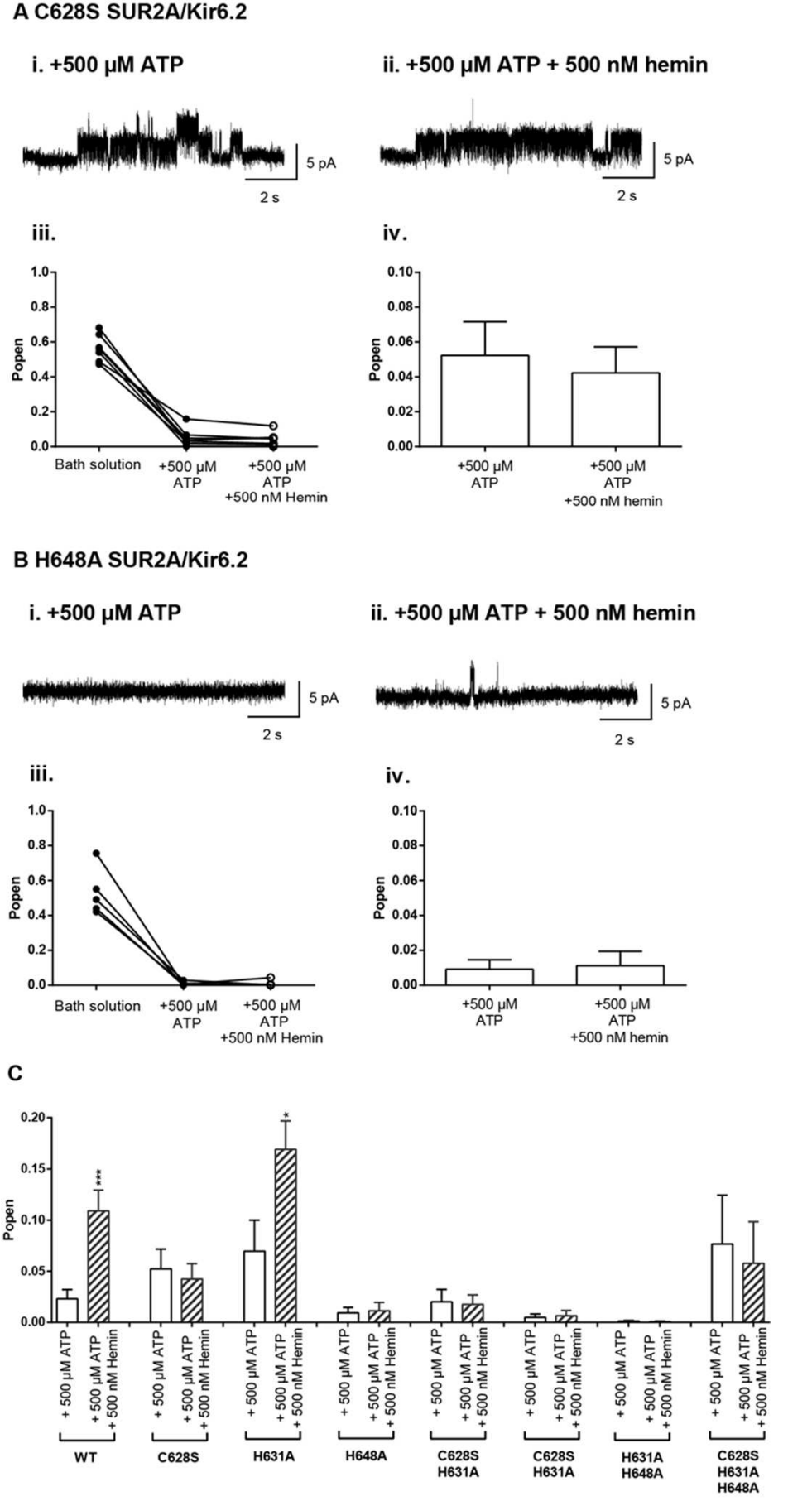
A C628S SUR2A/Kir6.2
i. +500 µM ATP
ii. +500 µM ATP + 500 nM hemin
5 pA
2 s
iii.
iv.
Popen
Bath solution
+500 µM ATP
+500 µM ATP +500 nM Hemin
B H648A SUR2A/Kir6.2
C
WT
C628S
H631A
H648A
C628S H631A
C628S H631A
H631A H648A
C628S H631A H648A

Figure 6

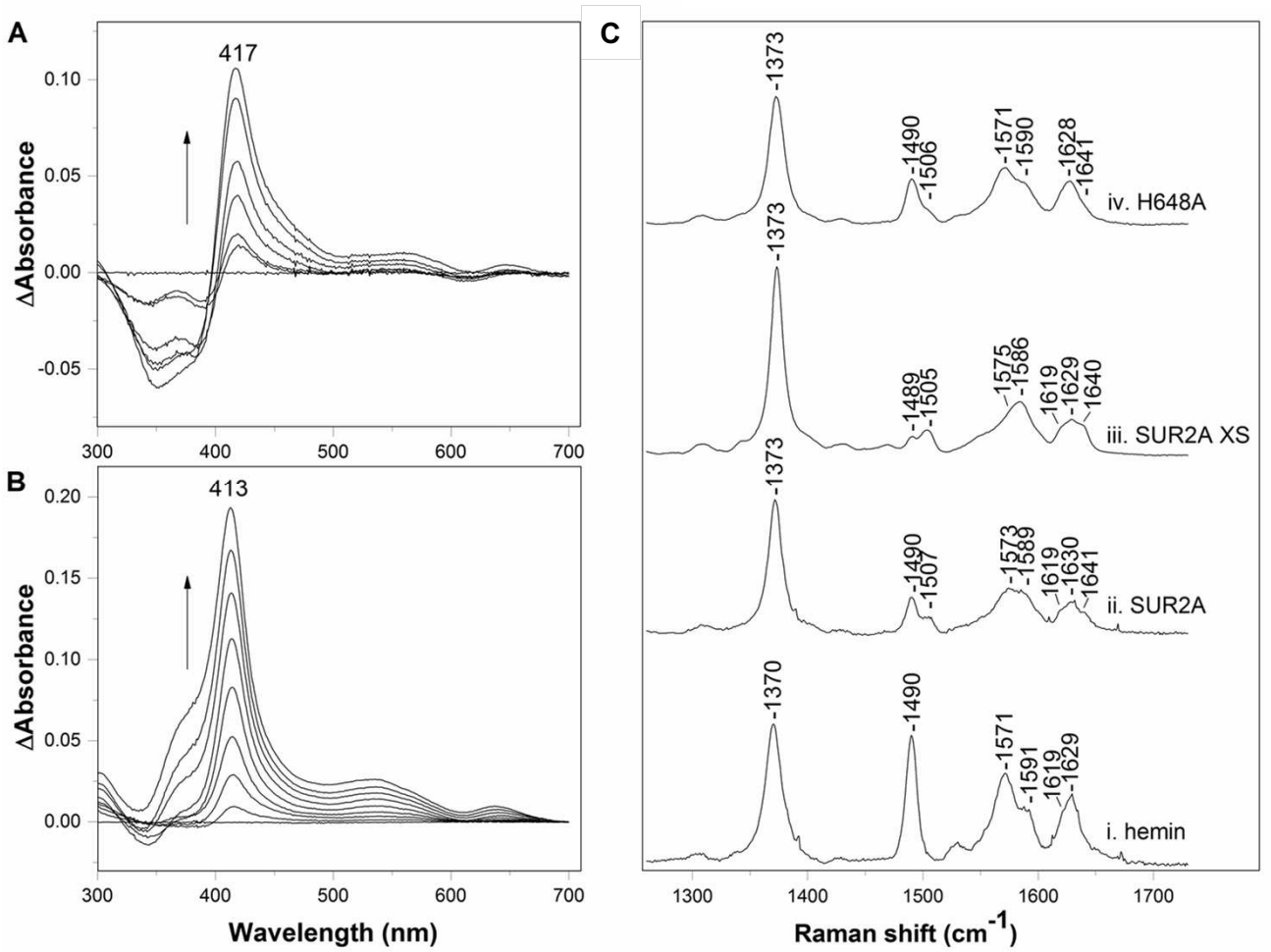
A
417
0.10
0.05
0.00
-0.05
ΔAbsorbance
300
400
500
600
700
B
413
0.20
0.15
0.10
0.05
0.00
ΔAbsorbance
300
400
500
600
700
Wavelength (nm)
C
-1373
-1490
-1506
-1571
-1590
-1628
-1641
iv. H648A
-1373
-1489
-1505
-1575
-1586
-1619
-1629
-1640
iii. SUR2A XS
-1373
-1490
-1507
-1573
-1589
-1619
-1630
-1641
ii. SUR2A
-1370
-1490
-1571
-1591
-1619
-1629
i. hemin
1300
1400
1500
1600
1700
Raman shift (cm-1)

Scheme 1

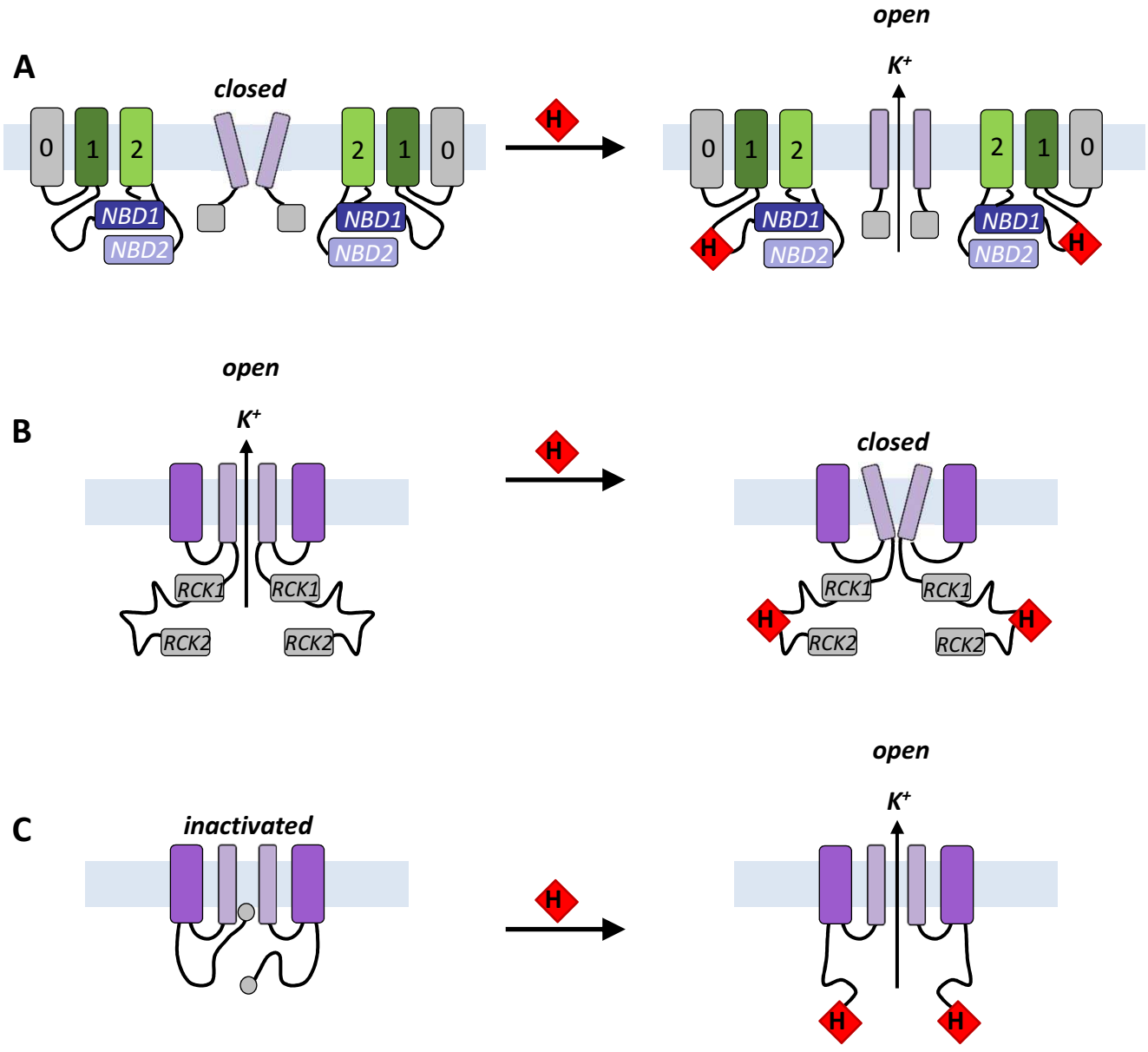
A
closed
open
K+
0
1
2
NBD1
NBD2
H
B
open
K+
closed
RCK1
RCK2
C
inactivated
open
K+

A heme-binding domain controls regulation of ATP-dependent potassium channels

Mark J. Burton[a,1], Sofia M. Kapetanaki[b,1], Tatyana Chernova[c], Andrew G. Jamieson[b], Pierre Dorlet[d], Jérôme Santolini[d], Peter C. E. Moody[e], John S. Mitcheson[a], Noel W. Davies[a], Ralf Schmid[a], Emma L. Raven[b,2], Nina M. Storey[a,2]

[a] Department of Molecular and Cell Biology, University of Leicester, Leicester, LE1 9HN, United Kingdom.

[b] Department of Chemistry, University of Leicester, Leicester, LE1 7RH, United Kingdom.

[c] MRC Toxicology Unit, Hodgkin Building, Lancaster Road, Leicester LE1 9HN, United Kingdom.

[d] Institute for Integrative Biology of the Cell (I2BC), CEA, CNRS, Univ Paris-Sud, Université Paris-Saclay, 91198, Gif-sur-Yvette cedex, France.

[e] Department of Molecular and Cell Biology and Henry Wellcome Laboratories for Structural Biology, University of Leicester, Leicester, LE1 9HN, United Kingdom.

SUPPLEMENTARY METHODS

Chemicals and reagents. Iron protoporphyrin IX (hemin, $C_{34}H_{32}ClFeN_4O_4$, FW 651.96 g/mol) was purchased from Sigma Aldrich. Aqueous stock solutions of hemin (which is in the ferric (+3) oxidation state) for spectroscopic and electrophysiology experiments were prepared by dissolving 1 mg of hemin in 0.1 M aqueous NaOH and then mixing for 10 min. The solution was clarified by centrifugation at 4000 g for 10 min and appropriate dilutions were made with corresponding buffers. All electrophysiology buffers with or without hemin also contained 1 mM reduced glutiathione (GSH). Aliquots of hemin were made fresh daily. Exact concentrations of hemin were calculated spectrophotometrically at 385 nm (ε_{385} = 58.4 $mM^{-1}cm^{-1}$) (42). In the electrophysiology experiments, it is not known whether the heme stays in the +3 oxidation state or whether (unknown) heme reductases convert the heme to ferrous within the intracellular environment. Protoporphyrin IX ($C_{34}H_{34}N_4O_4$, FW 562.66 g/mol), tin

protoporphyrin IX dichloride ($C_{34}H_{32}N_4O_4Sn•2Cl$, FW 750.30 g/mol) and zinc protoporphyrin ($C_{34}H_{32}N_4O_4Zn$, FW 626.0 g/mol) were purchased from Santa Cruz Technology (Dallas, USA) and stock solutions were made up in 0.1 mM NaOH at a concentration of 1 mM, P1075 and glibenclamide were from Tocris Bioscience, (Abingdon, England) and all other reagents were from Sigma-Aldrich (Dorset, England).

Isolation of cardiac myocytes. Cardiac myocytes were obtained from adult male Wistar rats (300-400 g) killed by stunning and cervical dislocation, a method approved under the UK Animals (Scientific Procedures) Act, 1986. The heart was removed within 1 minute and cannulated for retrograde perfusion at the aorta using a Langendorff apparatus. The single ventricular myocytes were isolated through enzymatic digestion with collagenase (type I) and protease (type XV) as described previously (43). The isolation procedure typically yielded 70 – 90% viable quiescent rod shaped myocytes. Following isolation myocytes were stored in Tyrode solution at room temperature (approximately 22 ^{o}C) at a density of approximately 0.4 million cells/ml and were used for experimentation within 10 hours.

Transfection and cell culture. Human embryonic kidney 293 (HEK293) cells were cultured on sterile glass cover slips in Minimum Essential Medium (MEM) (Life Technologies) with 10% Foetal Bovine Serum (FBS), 1% L-Glutamine and 1% streptomycin/penicillin and incubated at 37°C, 5% CO_2 for at least 24h before transfection or patch-clamp recordings were made. Transfection of HEK293 cells with plasmids encoding recombinant Kir6.2 and SUR2A was carried out using Lipofectamine 2000 (Life Technologies, Carlsbad, USA) 12-24 hours before recording. The rat Kir6.2-pIRES-eGFP and SUR2A-pCMV subunits were a generous gift from Dr David Lodwick, University of Leicester.

Electrophysiology. Conventional whole-cell patch clamp was used to record membrane currents from isolated cardiac myocytes with an Axopatch 200 amplifier. Signals were digitized using a Digidata 1440A interface, and records acquired and analysed using pClamp 10.3 software (Molecular Devices, Sunnyvale, CA, USA). Patch pipettes were made from thick-walled borosilicate glass (Harvard Apparatus, Edenbridge, UK) using a two-stage vertical puller (Narashige, Tokyo, Japan) to give electrode resistance between 2-5 MΩ and filled with a solution containing (mM): 140 KCl, 2 ATP, 0.1 ADP, 0.1 GTP, 1 $MgCl_2$, 10 HEPES, 5 BAPTA, titrated to pH 7.2 with NaOH. Cells were superfused with normal Tyrode solution containing (mM): 135 NaCl, 5 KCl, 0.33 NaH_2PO_4, 5 Na-pyruvate, 10 glucose, 1 $MgCl_2$, 2 $CaCl_2$, 10 HEPES, titrated to pH 7.4 with NaOH. P1075 and glibenclamide were from Tocris Bioscience, (Abingdon, England) and all other reagents were from Sigma-Aldrich (Dorset, England).

Single channel currents were recorded at 70 mV and records were sampled at 10 kHz and filtered at 2 kHz. To obtain single channel recordings the patch was excised in the inside-out configuration into a bath containing (mM): 30 KOH, 110 KCl, 10 EGTA, 1.2 $MgCl_2$, 1 $CaCl_2$, 5 HEPES, 1 reduced glutathione, pH 7.2. Pipettes were filled with a solution containing (mM): 140 KCl, 1.2 $MgCl_2$, 2.6 $CaCl_2$, 5 HEPES, pH 7.4. Open probability (P_{open}) was calculated by measuring the times, t_j, where current level corresponded to j = 0, 1, 2…N channels open. P_{open} will then be equal to $\left(\sum_{j=1}^{N} t_j j\right)/TN$, where N is the number of channels in the patch, estimated as the maximum number seen during high activity, and T is the duration of the recording. All experiments were conducted at room temperature (22 ± 1 °C). Data are presented as mean ± SEM of *n* experiments.

Prior to recording, a population of the ventricular myocytes were treated with 1 mM succinylacetone (SA) to inhibit heme synthesis and a population of myocytes were treated with hemin (500 nM) in the presence of bovine serum albumin (BSA) in a 1:1 molar ratio as described before (44) for 4 hours.

RNA extraction and Quantitative Real-Time PCR analysis. Treated and untreated cells at different time point were collected and total RNA was isolated by using TRI-reagent (Sigma-Aldrich). cDNA synthesis was carried out using random primers and Superscript II (Invitrogen). PCR primers were designed using the Primer Express v2.0 Software program (Applied Biosystems, Foster City, CA). Primers sequences were as follows: *Alas1* forward primer 5'-TCTTCCGCAAGGCCAGTCT-3', reverse primer 5'- AAGAGGCTGCTCAAGCCCA-3'; GAPDH forward primer 5'-CAGTGCCAGCCTCGTCTCAT-3'; reverse primer 5'-AGGGGCCATCCACAGTCTTC-3'.

Primers were designed to cross exon-exon boundaries and the concentration optimised (300-900 nM) to ensure that the efficiency of the target amplification and the efficiency of the endogenous reference amplification are approximately equal. PCR was performed using SYBR Green PCR Master Mix, primers and 100 ng of reverse transcribed cDNA in the ABI PRISM 7700 Sequence Detection System, the thermal-cycler protocol was: stage one, 50 °C for 2 min; stage two, 95 °C for 10 min; stage three, 40 cycles at 95 °C for 15 sec and 60 °C for 1 min. Each sample was run in triplicate. The CT (threshold cycle when fluorescence intensity exceeds 10 times the standard deviation of the baseline fluorescence) value for the target amplicon and endogenous control (GAPDH) were determined for each sample. Quantification was performed using the comparative CT method ($\Delta\Delta$CT). Data are presented as the mean ± S.D. (n = 3–4 for each group). Statistical significance was assessed as $P < 0.05$ using one-way analysis of variance.

Expression and purification of SUR2A NBD1. Wild type rat SUR2A NBD1 (S615-L933) coding sequences were subcloned in the pSUMODAVE vector using the NcoI and HindIII restriction sites. The pSUMODAVE vector was a kind gift of Mr. C. David Owen (University of St. Andrews) and Dr. David Roper (University of Warwick) (45). The resulting constructs of rat SUR2A NBD1 (S615-L933) containing a His6 tag followed by SUMO and then a TEV protease site were expressed in *E.coli* strain BL21 (DE3) with slight modifications to previously described procedures (46). Briefly, cell cultures were grown in LB Broth containing kanamycin (30 mg/ml) at 37 °C to an OD_{600} of 0.4. The incubation temperature was gradually decreased to 18 °C until the OD_{600} reached 0.8, at which point the expression of the protein was induced by addition of 0.2 mM IPTG. After 20 h the cells were harvested by centrifugation and the pellets were stored at -80 °C. Purification of SUR2A NBD1 (residues S615-L933) was carried out at 4 °C. Cells were thawed and resuspended in lysis buffer (20 mM Tris, pH 8.00, 100 mM L-Arg, 2 mM β-mercaptoethanol, 10 mM ATP, 10 mM $MgCl_2$, 5 mM imidazole, 0.2 % [v/v] Triton-X100, 10 % [v/v] glycerol, 2mg/ml deoxycholic acid, 1mg/ml lysozyme, 1 complete ULTRA Tablet, Mini, EASYpack [Roche]). The cell lysate was loaded onto a 5 ml Ni^{2+}-NTA (Qiagen) affinity column equilibrated with 20 mM Tris, pH 7.6, 150 mM NaCl, 10 mM ATP, 10 mM $MgCl_2$, 2 % [v/v] glycerol, and 5 mM imidazole. After washing with equilibration buffer the His_6-SUMO-protein was eluted with 20 mM Tris, pH 7.3, 150 mM NaCl, 2 mM ATP, 2 mM $MgCl_2$, 2 % [v/v] glycerol, and 400 mM imidazole. The elution fractions were immediately diluted 3-fold into a buffer containing 20 mM Tris, pH 7.3, 2 mM ATP, 2 mM $MgCl_2$, 5 mM β-mercaptoethanol and 2 % [v/v] glycerol. Imidazole was removed and the His_6-SUMO tag was cleaved from NBD1 with a His-tagged TEV-protease during overnight dialysis. The His_6-SUMO tag and His-tagged

TEV protease were removed by reverse Ni^{2+}-NTA affinity column and SUR2A NBD1 was purified to homogeneity with size exclusion chromatography (Superdex 75, GE Healthcare) using 20 mM Tris, pH 7.3, 150 mM NaCl, 2 mM ATP, 2 mM $MgCl_2$, 5 mM β-mercaptoethanol, and 2 % [v/v] glycerol. Purity of the final preparations was assessed by SDS-PAGE. Protein concentration was determined by Bradford protein assay.

Peptide synthesis. The peptides LPFESCKKHTGVQSKPINRKQPGRYHLDNYE and LPFESSKKATGVQSKPINRKQPGRFALDNFE (with N-terminal acetylation and C-terminal amidation, purity >95%) were purchased from Thermo Fisher Scientific.

Spectroscopy of hemin-bound species:

i.Difference absorption spectroscopy

Solutions of ferric hemin (ε_{385} = 58.4 $mM^{-1}cm^{-1}$ (42)) were prepared by dissolving solid hemin in 0.1 M NaOH. The hemin binding properties of the peptides and SUR2A were studied by difference absorption spectroscopy using a double beam spectrophotometer (Perkin Elmer Lambda 40). Hemin (50 - 400 µM) was added step-wise to the sample cuvette containing the peptides (10 µM) or SUR2A(S615-L933) (7 µM) in 50 mM phosphate, 50 mM NaCl pH 8.00 and to the reference cuvette containing the peptides/protein-free buffer. Spectra were recorded after each hemin addition.

ii.Resonance Raman Spectroscopy

Samples (50 µL) of ferric SUR2A(S615-L933), H648A and C628S mutants solutions in 50 mM Hepes, 50 mM NaCl pH 7.5 at 90-120 µM were prepared in quartz EPR tubes and disposed in a homemade spinning cell, at room temperature, to avoid local heating and to prevent photodissociation and degradation. Raman excitation at 413.1 nm was achieved with a laser power of ∼10 mW from a Kr^+ laser (Coherent I-302). Resonance Raman spectra were recorded using a modified single-stage spectrometer (Jobin-Yvon T64000, HORIBA Jobin Yvon S.A.S., Chilly Mazarin, France) equipped with a liquid N_2-cooled back-thinned CCD detector. Stray scattered light was rejected using a holographic notch filter (Kaiser Optical Systems, Ann Arbor, MI). Spectra correspond to the average of three different 1 h accumulations. The spectral accuracy was estimated to be ±1 cm^{-1}. The spectral resolution was ∼3 cm^{-1}. Baseline correction was performed using GRAMS 32 (Galactic Industries, Salem, NH).

iii.EPR Spectroscopy

X-Band (9.4 GHz) EPR spectra were recorded on a Bruker ELEXSYS 500 spectrometer equipped with a standard TE cavity (Bruker) and an Oxford Instruments continuous flow liquid helium cryostat interfaced with a temperature control system. Samples (100 μl) of ferric SUR2A(S615-L933) and site-directed mutants were prepared in 50 mM Hepes, 50 mM NaCl pH 7.5 at a concentration of 100 uM, and transferred to quartz EPR tubes.

Bioinformatics analyses. *Sequence Analysis.* The SUR2A sequence (UniProt id: sp|O60706|ABCC9_HUMAN) was retrieved from the UniProt database and used as input for a NCBI-BLAST sequence similarity search against SwissProt. From the BLAST results twelve human homologs of the ATP-binding cassette, sub-family C (CFTR/MRP) were extracted using taxid:9606 as species filter. These sequences were aligned with MAFFT and visualised in Jalview. The domain structure of SUR2A was analysed considering Pfam domains as identified by InterProScan.

Homology Modelling. An HHPred search against pdb identified the structures of the *C. elegans* multidrug resistance protein PGP-1 (PDB-id: 4F4C, 20 % pairwise sequence identity (36)) and the mouse MRP-1A protein (PDB-id: 3G5U, 18 % pairwise sequence identity (47)), both covering the transmembrane domains, as plausible templates for modelling SUR2A. The HHPred target-template sequence alignment was adjusted for consistency with the 4F4C structure and used as input for model generation in Modeller 9v4. 50 models were generated and ranked by the DOPE score, and the best ranking model was used for structure analysis and visualisation in pymol.

FIGURE S1. (*A*) Schematic representation of cardiac sarcolemmal K_{ATP} channel structure; four SUR2A subunits assemble with four pore-lining Kir6.2 subunits to form an octameric channel structure. Highlighted in red is the disordered protein region which contains the motif $CXXHX_{16}H$ leading into nucleotide binding domain 1 (NBD1). *(B)* Multiple sequence alignment of the human ATP-binding cassette sub-family C (CFTR/MRP) proteins using the CLUSTAL colour scheme. Shown is the section of the alignment covering the $CXXHX_{16}H$ motif and parts of the adjacent transmembrane domain 1 (TMD1) and nucleotide binding domain 1 (NBD1). The SUR2A rat sequence was added for comparison.

FIGURE S2. Heme increases cardiac K_{ATP} currents. (*A*) Whole-cell recording of K_{ATP} currents (current amplitudes are normalised to cell capacitance and expressed as pA/pF) from an isolated ventricular myocyte. Currents were recorded at 0 mV, and P1075 (10 μM) and glibenclamide (10 μM) were bath applied as indicated by the bar. (*B*) Whole-cell recording of K_{ATP} currents, as above, with addition of hemin (500 nM) as indicated by the bar. (*C*) Concentration response curve for hemin induced increase in the K_{ATP} current in isolated ventricular myocytes. Experiments were repeated, for the data set for log [hemin] -9, -8 and -7.5, n = 6; -7 and -6.5, n = 7; and -6 n = 8. Whole-cell recordings of K_{ATP} currents from isolated ventricular myocytes from a holding potential of 0 mV, and P1075 (10 μM), with (*D*), zinc protoprorphyrin IX (ZnPP) (500 nM) or (*E*), $FeSO_4$ (500 nM) and glibenclamide (10 μM) were bath applied as indicated by the bar. (*F*) Summary graph showing the change in K_{ATP} current normalised to P1075 current of ventricular myocytes either untreated (control = 1) (n = 6) or treated with hemin (n = 7), protoporphyrin IX (PP) (n= 3) zinc protoprorphyrin IX (ZnPP) (n = 3), tin protophorphyrin IX (SnPP) (n = 4), and $FeSO_4$ (n = 5). *** $P \leq 0.001$ ** $P \leq 0.01$ *vs*. control. ANOVA, Dunnett's post-hoc test.

FIGURE S3. Inhibition of heme synthesis causes a reduction in K_{ATP} currents recorded from adult rat ventricular myocytes. A) Q-PCR, normalised to the housekeeping gene GAPDH, showed an up-regulation of ALAS-1 in response to inhibition of heme synthesis with SA (1 mM for 4 hours). * $P \leq 0.05$, n = 4, significantly different from control with Student's t-test. B) i. Representative whole-cell trace of normalised K_{ATP} current (pA/pF) in response to P1075 (10 μM) compared to (ii) a current recording from a myocytes pre-treated with SA (1 mM) for 4 hours. C) Mean peak current elicited by P1075 for control myocytes and those incubated in SA for 4 hours illustrated a significant decrease from 21.8 ± 2.5, n = 28 to 10.7 ± 1.8, n = 8 (unpaired t-test *$P < 0.05$).

FIGURE S4. Heterologously expressed K_{ATP} channels are activated by heme. (*A*) Patches were exposed to 0 ?M ATP solution (*i*), locally perfused with 500 µM ATP (*ii*) and 500 µM ATP plus 500 nM hemin (*iii*). Exposure to the K_{ATP} blocker glibenclamide (50 µM) inhibited channel activity (*iv*). (*B*) P_{open} values are plotted and (*C*) mean increases in P_{open} are observed from 0.023 ± 0.009, n = 9 for +500 µM ATP alone to 0.109 ± 0.020, n = 9, (*** $P \leq 0.001$) for +500 ATP + 500 nM hemin. (*D*) Macropatch recordings from K_{ATP} channels illustrate increase in channel current at all potentials with the presence of 500 nM hemin, n = 3.

FIGURE S5. High-frequency resonance Raman spectra of (i) hemin, (ii) the SUR2A(S615-L933)-hemin immediately after hemin addition, (iii) the SUR2A(S615-L933)-hemin complex 4 hours after hemin addition.

FIGURE S6. X-band EPR spectra of (i) hemin, (ii) SUR2A(S615-L933)-hemin complex, (iii) SUR2A(S615-L933)-hemin complex (4-5 fold excess of SUR2A), (iv) H648A-hemin complex, (v) C628S-hemin complex, and (vi) H631A-hemin complex. The signals indicated by * and ** indicate an artefact signal and minor Cu(II) contamination, respectively. Experimental conditions: microwave frequency 9.39 GHz, microwave power 1mW (left panel) and 0.25 mW (right panel), 1 scan (left panel) and 4 scans (right panel) per spectrum, field modulation amplitude 2 mT, field modulation frequency 100 kHz, temperature 20K, [heme]=100µM.

FIGURE S7. Blumberg-Peisach correlation diagram including various heme proteins. The figure shows a correlation between the strength of the axial field in units of the spin−orbit coupling constant λ (x-axis) and the ratio of the rhombic and axial crystal field parameters (y-axis). SUR2A lies in the region designated for Cys(S^-)/X heme coordination environment (15).

Figure S1

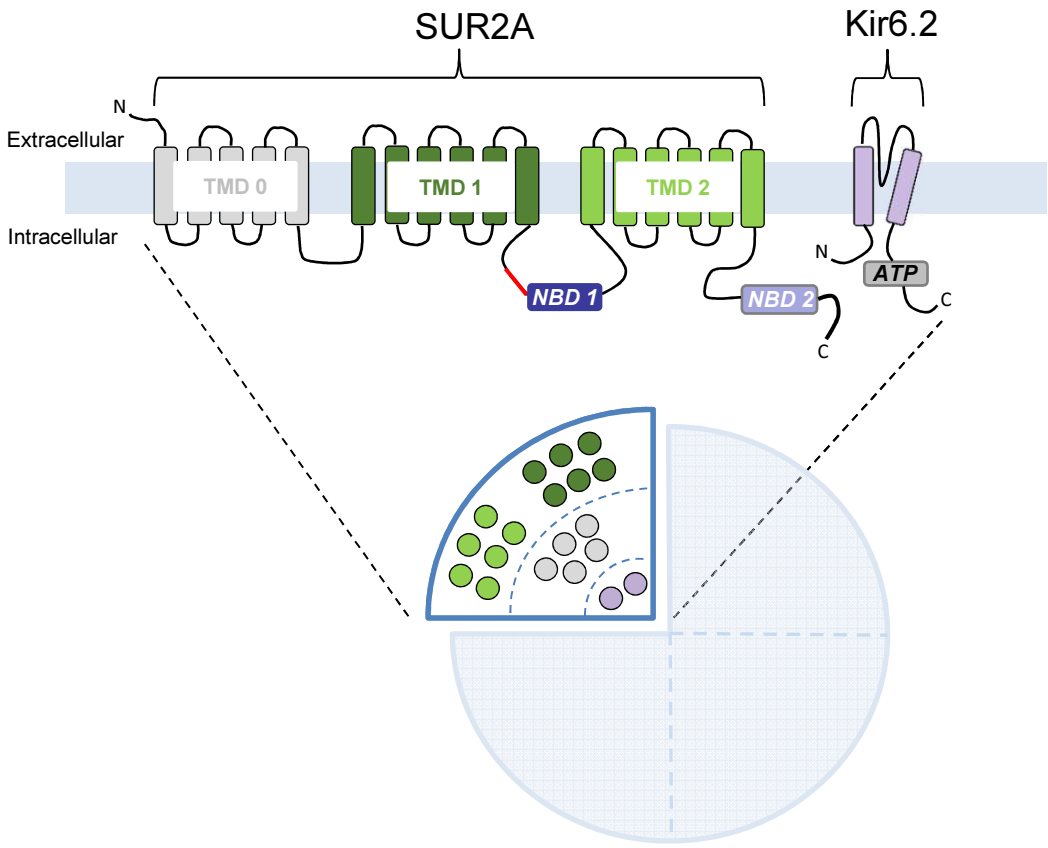
SUR2A
Kir6.2
N
Extracellular
Intracellular
TMD 0
TMD 1
TMD 2
NBD 1
NBD 2
N
ATP
C
C

Figure S2

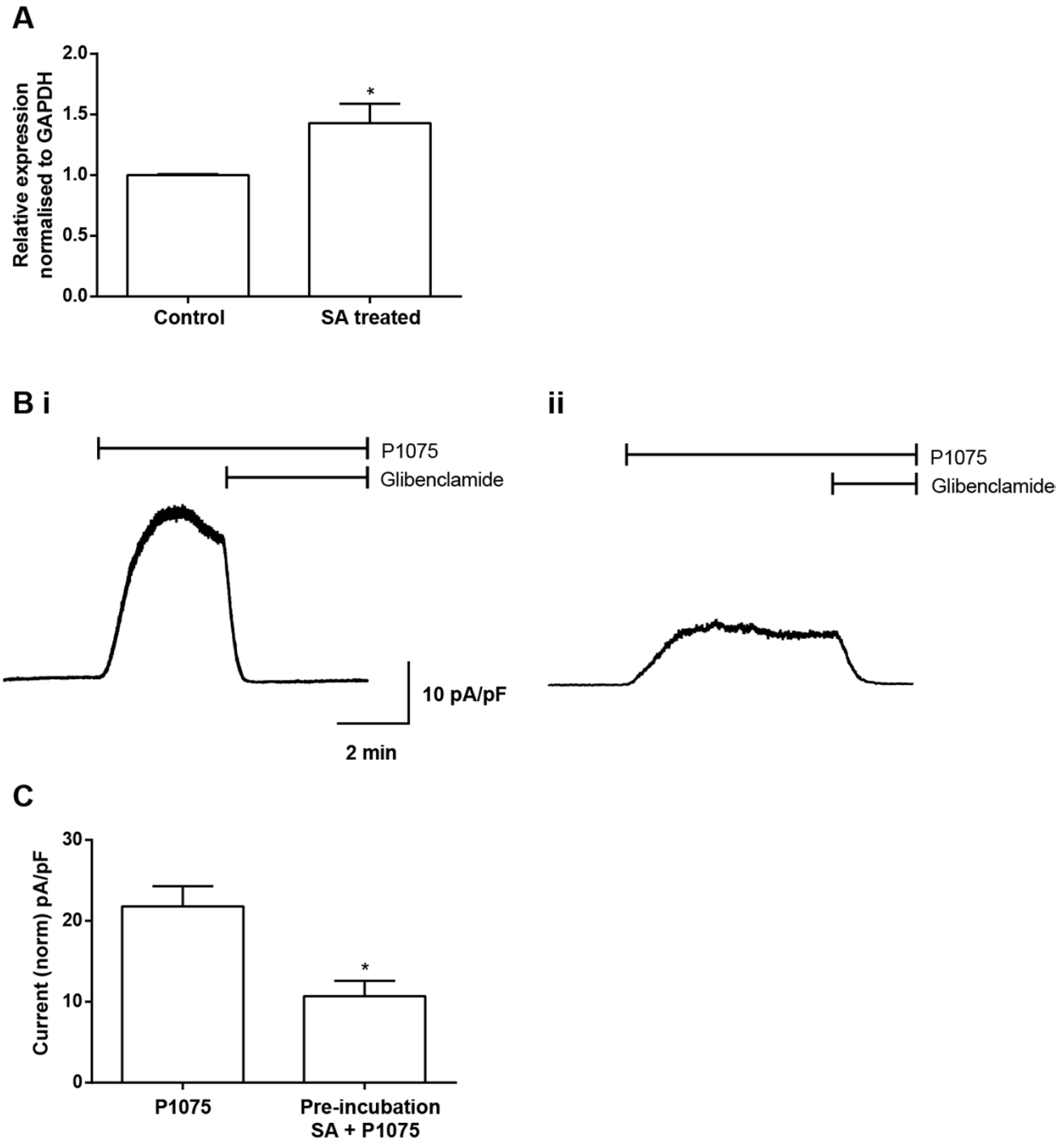
A
Relative expression normalised to GAPDH
2.0
1.5
1.0
0.5
0.0
*
Control
SA treated
B i
P1075
Glibenclamide
10 pA/pF
2 min
ii
P1075
Glibenclamide
C
Current (norm) pA/pF
30
20
10
0
*
P1075
Pre-incubation SA + P1075

Figure S3

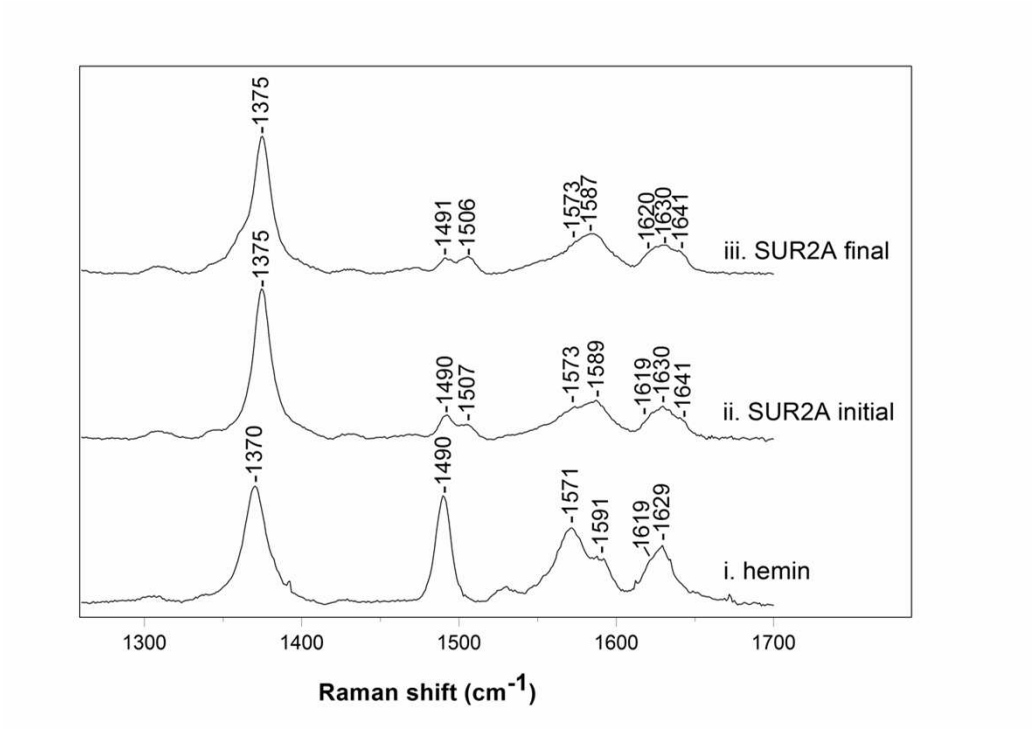
1375
1491
1506
1573
1587
1620
1630
1641
iii. SUR2A final
1375
1490
1507
1573
1589
1619
1630
1641
ii. SUR2A initial
1370
1490
1571
1591
1619
1629
i. hemin
1300
1400
1500
1600
1700
Raman shift (cm-1)

Figure S4

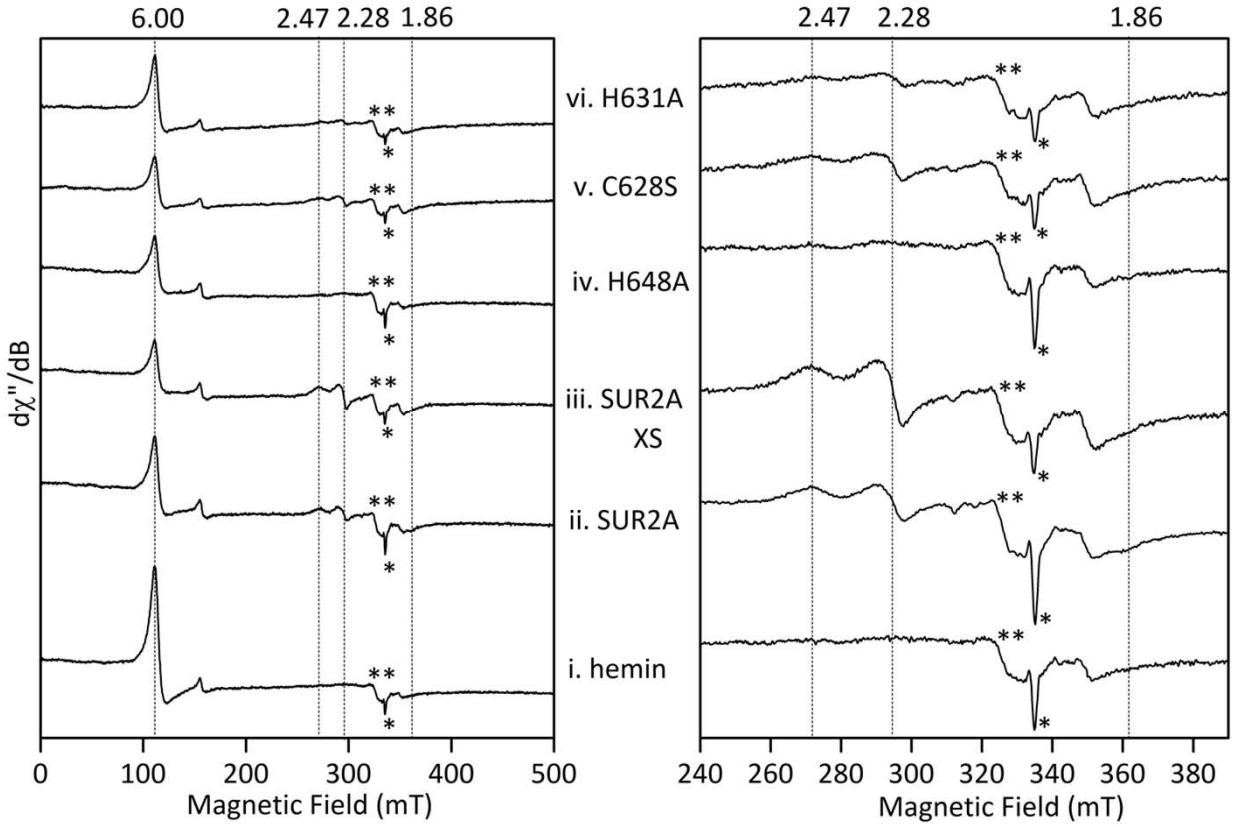
6.00
2.47 2.28 1.86
vi. H631A
v. C628S
iv. H648A
iii. SUR2A XS
ii. SUR2A
i. hemin
dχ''/dB
0 100 200 300 400 500
Magnetic Field (mT)
2.47 2.28 1.86
240 260 280 300 320 340 360 380
Magnetic Field (mT)

Figure S5

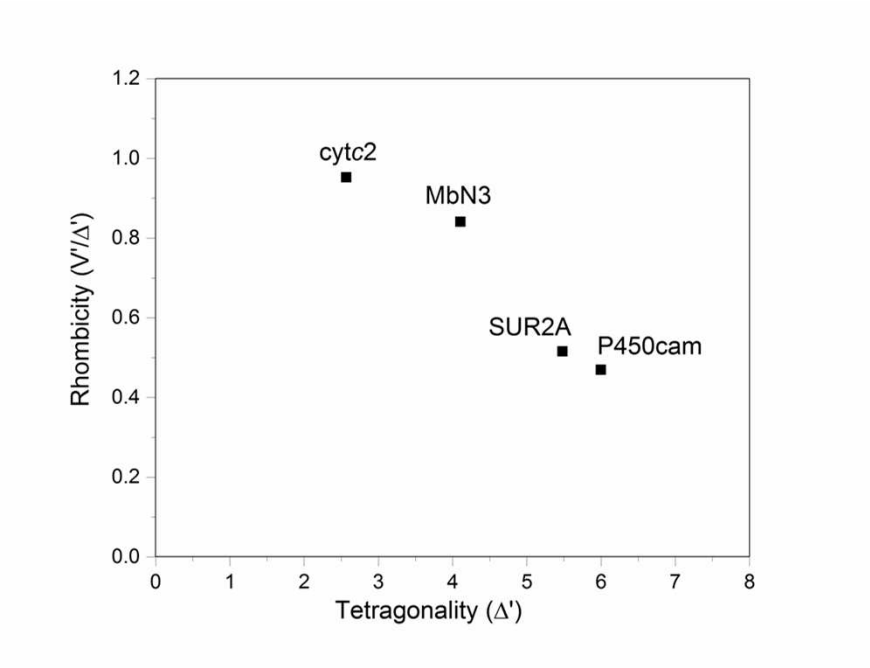
1.2
1.0
0.8
0.6
0.4
0.2
0.0
Rhombicity (V'/Δ')
cytc2
MbN3
SUR2A
P450cam
0
1
2
3
4
5
6
7
8
Tetragonality (Δ')